Taming charge transport in semiconducting polymers with branched alkyl side chains.

Bob C. Schroeder, Tadanori Kurosawa, Tianren Fu, Yu-Cheng Chiu, Jaewan Mun, Ging-Ji Nathan Wang, Xiaodan Gu, Leo Shaw, James W. E. Kneller, Theo Kreouzis, Michael F. Toney, and Zhenan Bao*

Dr. B. C. Schroeder, Dr. T. Kurosawa, T. Fu, Dr. Yu-Cheng Chiu, J. Mun, G-J. N. Wang, Dr. X. Gu, L. Shaw, Prof. Z. Bao
Department of Chemical Engineering, Stanford University, 443 Via Ortega, Stanford, California 94305, United States.
E-mail: zbao@stanford.edu

Dr. X. Gu, Dr. M. F. Toney
Stanford Synchrotron Radiation Lightsource, SLAC National Accelerator Laboratory, Menlo Park, California 94025, United States.

J. W. E. Kneller, Dr. T. Kreouzis
Materials Research Institute and School of Physics and Astronomy, Queen Mary University of London, Mile End Road, London E1 4NS, United Kingdom.

Dr. B. C. Schroeder
Materials Research Institute and School of Biological and Chemical Sciences, Queen Mary University of London, Mile End Road, London E1 4NS, United Kingdom.

Dr. T. Kurosawa,
Department of Advanced Materials Science, School of Frontier Sciences, University of Tokyo, 5-1-5 Kashiwanoha, Kashiwa, 277-8561 Chiba, Japan.

Prof. Y-C. Chiu
Department of Chemical Engineering and Materials Science, Yuan Ze University, 135 Yuandong Rd, Zhongli District, Taoyuan City, Taiwan.

Prof. X. Gu
School of Polymers and High Performance Materials, University of Southern Mississippi, 118 College Drive, Hattiesburg, Mississippi 39406, United States.

The solid-state packing and polymer orientation relative to the substrate are key properties to control in order to achieve high charge carrier mobilities in organic field effect transistors (OFET). Intuitively, shorter side chains are expected to yield higher charge carrier mobilities

because of a denser solid state packing motif and a higher ratio of charge transport moieties, however our findings suggest that the polymer chain orientation plays a crucial role in high-performing diketopyrrolopyrrole-based polymers. By synthesizing a series of DPP-based polymers with different branched alkyl side chain lengths, we show that the polymer orientation depends on the branched alkyl chain lengths and that the highest carrier mobilities are obtained only if the polymer adopts a mixed face-on / edge-on, which allows the formation of three-dimensional carrier channels in an otherwise edge-on-oriented polymer chain network. Time-of-flight measurements performed on the various polymer films support this hypothesis by showing higher out-of-plane carrier mobilities for the partially face-on oriented polymers. Additionally, we mimic a favorable morphology by blending a "face-on" polymer into an exclusively "edge-on" oriented polymer, resulting in higher charge carrier mobilities and opening up a new avenue for the fabrication of high performing OFET devices.

1. Introduction

Over the course of the last twenty years, the field of semiconducting polymers has experienced huge developments, both in the fields of physics and materials chemistry. Whereas physicists were driven to understand the underlying physical properties of this new class of electronic materials, chemists primarily focused on developing new and ever more innovative conjugated materials. However, as novel organic semiconductors became more and more challenging to synthesize, physical properties like charge carrier mobilities started to stagnate,[1] and the chemists' focus shifted from synthesizing a plethora of different conjugated materials to a more targeted approach to attempt to improve the physical properties of known organic semiconductors with modest chemical alteration. The most striking example of this development is the increasing interest in the alkyl side chains, which are no longer regarded

primarily as strictly solubilizing groups, but as attractive functional groups that can have a profound impact on the physical properties of polymer semiconductors.[2]

In contrast to the conjugated backbone with its delocalized π-bonds, the alkyl side chains do not directly contribute to the charge transport in organic semiconductors but instead act as insulating material. Long and branched alkyl side chains might provide better solubility, but compromise effective molecular packing and thus charge carrier mobilities in organic field effect transistors (OFET).[3] In contrast, short and linear alkyl side chains enhance crystallinity and π-π interactions, usually lead to higher charge carrier mobilities but at the expense of material processability.[4] Therefore, it is of utmost importance to find the right balance between device performance and processability. The side chains, however, not only influence crystallinity and solubility but also long-term device stability,[5] mechanical properties,[6] opto-electronic properties,[7] and molecular packing and orientation relative to the substrate.[8]

Early studies on conjugated polymers came to the conclusion that an edge-on orientation of the polymer chains with respect to the substrate is beneficial for efficient charge transport in thin film transistors.[9] This assumption is true for polymers that adopt a highly ordered lamellar packing motif, like regioregular polythiophenes,[10] because the edge-on orientation allows the two fastest charge transport directions (*i.e.* along the π-π stacking direction ($\sim 10^{-2}$ to 10^{-3} $cm^2.V^{-1}.s^{-1}$) and the conjugated backbone axis (~ 1 to 10^{-1} $cm^2.V^{-1}.s^{-1}$)) to align parallel to the substrate, thus facilitating charge transport between electrodes in conventional transistor architectures.[11] In recent years, a series of so called "push-pull" polymers emerged that showed exceptionally high charge carrier mobilities in OFET devices [12] without adopting a highly ordered edge-on orientation. In contrast, those donor-acceptor materials showed a strong preference for face-on orientations and relatively poor long-range order. Recently, two complementary concepts emerged to rationalize why rather poorly ordered semiconducting polymers are able to achieve

charge carrier mobilities comparable to amorphous silicon ($\sim 1 \text{ cm}^2.\text{V}^{-1}.\text{s}^{-1}$). One prerequisite to achieve high charge carrier mobilities was found to be minimal conformational disorder along the conjugated backbone.[13] The improved backbone co-planarity leads to the formation of 1-D, high-mobility charge transport pathways in the polymer films, which are not tremendously affected by an overall lack of long range order in the semiconducting polymer. Furthermore, Noriega *et al.* stipulated that a second requirement for high charge carrier mobility in conjugated polymers is high molecular weight.[14] Smaller, more ordered polymer aggregates in a semiconducting polymer film favour intra- and intermolecular charge transfer at the molecular level, but in order to translate into efficient macroscopic charge transport, those domains have to be interconnected, which can only be achieved by the presence of high molecular weight polymer molecules acting as tie chains.

These two concepts rationalize why relatively poorly ordered semiconducting polymers are able to achieve exceptionally high carrier mobilities. However, they focus mainly on the nature of the conjugated backbones and not so much on the influence of the side chains. In this work, we are primarily interested in the influence of the side chains on the molecular packing and how this affects hole carrier mobilities in OFET devices.

2. Results & discussion

In order to conduct a valid comparison, we minimized the number of variables: the conjugated backbone was first chosen before the side chain geometry and length, whilst the molecular weight of all polymers was identical, ensuring that only one parameter was modified at a time. 2,5-dialkyl-3,6-di(thiophen-2-yl)-2,5-dihydro-pyrrlo[3,4-*c*]pyrrole-1,4-dione (**DPPT**) - containing polymers are one of the most explored classes of semiconducting in recent years, mainly because of their good solution processability and charge carrier mobilities achieved in OFETs.[15] In addition, the thienyl-flanked **DPP** unit is coplanar due to minimal steric

hindrance and favourable hydrogen bonding interactions between the β-hydrogen on the thiophene and the oxygen atom of the lactam unit.[16] Copolymerizing the **DPPT** core with the linear thieno[3,2-*b*]thiophene (**TT**)[17] moiety further enhances the backbone co-planarity and favours 1-D charge transport along the polymer backbone. One of the key benefits of polymer semiconductors is their solution processability,[18] and in order to ensure sufficient solubility, the conjugated **DPPT-TT** backbone was decorated with branched alkyl side chains. However, the high carrier mobilities often observed in **DPPT-TT** polymers are in part owed to strong intermolecular π-π interactions as a result of short π-π stacking distances. To further amplify those beneficial interactions, we moved the branching point of the alkyl side chain from the typical beta position to the delta position.[19] The last parameter we tuned is the length of the two different alkyl branches on the side chain. Instead of using commercially available precursors (*i.e.* 2-octyl-1-dodecanol), the branched side chains were synthesized from scratch, allowing us to keep one branch at constant length (decyl-) and systematically vary the length (from hexyl- to tetradecyl-) of only the second branch.

The synthetic route towards the new side-chains and **DPPT** containing polymers is presented in Scheme 1. Commercial 1,3-propanediol (**1**) was monoprotected with a benzyl group, and the remaining hydroxyl group was converted into the corresponding bromide (**3**) via Appel reaction.[20] The Grignard reagent of the benzyloxybromide (**3**) was reacted with undecanoyl chloride in the presence of a catalytic amount of iron (III) acetylacetonate to yield selectively the γ-benzyloxyketone **4**.[21] The ketone was used as the starting material for the synthesis of the various branched side chains with different alkyl lengths, which were introduced via Grignard reaction and subsequent dihydroxylation of the tertiary alcohol (**5a-e**). A mixture of various constitutional isomers (**6a-e**) was recovered, which were reduced with hydrogen to the corresponding alcohols (**7a-e**) in quantitative yields. The hydroxyl group was substituted with an iodide, and the recovered alkyl iodides (**8a-e**) were introduced onto the **DPP** core. The

highly soluble alkylated **DPP** moieties (**9a-e**) were dibrominated with *N*-bromosuccinimide before being polymerized via palladium catalysed Stille coupling with 2,5-bis(trimethylstannyl)thieno[3,2-*b*]thiophene under microwave heating conditions. End-group effects and residual metal impurities can have significant effects on device performance by not only acting as charge traps but also because reactive end-groups and metal nanoparticles compromise the long term stability of semiconducting polymers.[22] To exclude these undesirable effects from this study, all **C$_x$C$_{10}$DPPT-TT** polymers were end-capped with phenyl groups and residual palladium was chelated with (*E*)-N,N-diethyl-2-phenyldiazene-1-carbothioamide.[23] The crude polymers were further purified by extensive Soxhlet extractions in methanol, acetone and hexane (24 h each) before being recovered with chloroform and slowly precipitated into methanol. The detailed polymer synthesis and purification procedures are available from the Supporting Information. All **C$_x$C$_{10}$DPPT-TT** polymers were recovered with excellent molecular weights, reasonably narrow weight dispersities (Đ$_w$), and high number-average degrees of polymerization (DP$_n$). The molecular weights are summarized in Table 1, and the corresponding size-exclusion chromatograms are provided in the Supporting Information. All polymers showed exceptionally high solubilities in common organic solvents at room temperature—even the **C$_6$C$_{10}$DPPT-TT** with the shortest 4-hexyltetradecyl side chain was readily soluble in chloroform at room temperature.

The UV-*vis.* absorption spectra of all polymers were measured in dilute chlorobenzene solution (~ 10^{-6} M) and thin-film (**Figure 1**). Both in solution and in the solid state, the **C$_x$C$_{10}$DPPT-TT** polymers present two distinct absorption bands, archetypal for donor-acceptor polymers. The more intense of the two bands at 800 nm originates from strong intramolecular coupling between the donor and acceptor moieties in the polymer backbone, whereas the weaker band at higher energies (450 nm) is associated with the π-π* transition. Unsurprisingly, the absorption features of all **C$_x$C$_{10}$DPPT-TT** polymers are nearly identical in solution. Due to the

dilute nature of the polymer solutions, the electronic transitions are mainly governed by the identical conjugated backbones and not affected significantly by intra-/interchain polymer aggregation in solution. The absorption maximum of **C_6C_{10}DPPT-TT** was measured at 834 nm and blue shifts towards 825 nm for **$C_{14}C_{10}$DPPT-TT** as the side chains elongate. In the solid state, the differences between the various absorption spectra are more apparent. The absorption maxima are hardly affected by the different alkyl side chains and located at around 828 nm. Interestingly, the vibrational peak (0-1) around 700 nm is altered by the nature of the different side chains and is slightly more intense for the polymers with the shorter side chains, **C_6C_{10}DPPT-TT** and **C_8C_{10}DPPT-TT**. Compared to the solution spectra the intense intramolecular charge transfer transition (ICT), centred around 800 nm, broadens by around 20 nm, a phenomenon commonly observed for **DPP** polymers.[24]

The ionization potentials were measured by cyclic voltammetry (CV) on thin polymer films, and the voltammograms are provided in the supporting information (**Figure S1**). The ionization potentials of **C_xC_{10}DPPT-TT** polymers were found to be -5.2 eV, and by adding the optical bandgap of around 1.3 eV, the electron affinity was estimated to be around -3.9 eV. Even though the different side chain lengths are expected to have an influence on the molecular packing in the solid state—which in return has been shown in the past to influence the frontier energy levels [3b, 25]—no differences could be observed for the various polymers in this case. According to thermal gravimetric analysis (TGA), the **C_xC_{10}DPPT-TT** polymers present excellent thermal stability, and significant degradation was only observed at temperatures exceeding 400°C (**Figure S2**). Differential scanning calorimetry (DSC) experiments were performed within the temperature range of –80°C to 300°C to gain a better understanding of the materials properties and the side chain influence thereon. Detailed DSC traces over the full temperature range are provided in the Supporting Information (**Figure S3**), and an enlargement of the sub-zero temperature range is depicted in **Figure 2**. Intuitively, one would expect the

polymers with shorter side chains to be more crystalline than their counterparts with longer alkyl chains. However, no obvious phase transitions, related to polymer chain melts, were observed at elevated temperatures, but the different C_xC_{10}DPPT-TT polymers unveiled significantly different behaviour at low temperatures. For the three polymers with the shortest side chains (C_6C_{10} to $C_{10}C_{10}$), no obvious first-order transition associated with side chain melting could be identified. The identified transitions in the range of –56 to –58°C strongly resemble in shape and intensity second-order transitions associated with the glass transition temperatures of the side chains.[26] The absence of side chain melting peaks is particularly surprising in the case of $C_{10}C_{10}$DPPT-TT polymer, for which one could have expected a more "crystalline" side chain arrangement because of the higher symmetry of the 4-decyltetradecyl side chain. However, it was only for the DPP-TT polymers with the longest side chains ($C_{12}C_{10}$ to $C_{14}C_{10}$) that clear side chain melts were observed at –43°C and –24°C, respectively.

Bottom-gate, top-contact (BGTC) field effect transistors (OFETs) were fabricated to probe the charge transport properties of the various C_xC_{10}DPPT-TT polymers and to investigate how charge transport might be influenced by the side chain architecture. Detailed device fabrication procedures, as well as transfer curves and output characteristics, are outlined in the Supporting Information. In **Figure 2b**, the measured hole mobilities are plotted as a function of side chain length. Intuitively, one would expect the hole mobility to decrease with increasing side chain lengths. However, this trend was only partially confirmed for the C_xC_{10}DPPT-TT polymer series. C_6C_{10}DPPT-TT exhibited a hole mobility of 2.10 ± 0.13 cm^2.V^{-1}.s^{-1} which hardly increased to around 2.5 cm^2.V^{-1}.s^{-1} for the polymers bearing the C_8C_{10} and the $C_{10}C_{10}$ side chains respectively. This is particularly surprising considering the high symmetry of the $C_{10}C_{10}$ side chain, for which a higher degree of order, and consequently higher charge carrier mobilities, might be expected. The highest hole mobilities, however were recorded for the $C_{12}C_{10}$DPPT-TT polymer (3.69 ± 0.42 cm^2.V^{-1}.s^{-1}), while a stark drop in average mobility

(1.38 ± 0.21 cm^2.V^{-1}.s^{-1}) was observed for the polymer with the longest side chain, **C$_{14}$C$_{10}$DPPT-TT**. It is noteworthy that many high mobility semiconducting polymers show non-linear behaviour when the square root of the current is plotted versus the applied gate voltage, especially in bottom gate device architectures using self-assembled monolayers to modify the SiO2 gate dielectric.[27] The presented **C$_x$C$_{10}$DPPT-TT** polymers herein are no exception, especially at higher negative gate voltages (< -60 V) (**Figure 3**). The origins of the observed nonlinear drain currents are most likely related to interfacial effects between the dielectric, the organic semiconductor, and the electrodes.[28] The proper extraction of charge carrier mobilities is under debate at the moment, and certain scrutiny should be applied to not systematically overestimate mobilities in organic semiconductors.[29] Uemura *et al.* recently showed that "intrinsic" carrier mobilities can be accurately extracted from non-linear transfer curves by means of gated four-point-probe (gFPP) and transmission line measurements (TLM).[30] However because the primary aim of this work is to establish a relationship between the side chain nature, the molecular packing and the charge transport properties of **DPP**-based polymers and not the achievement of high hole mobilities, we refrain from using such mobility extraction techniques. Given the weak non-linearity observed in the transfer curves of the different **C$_x$C$_{10}$DPPT-TT** polymers (**Figure 3**) and the identical fabrication procedures, we assume that the extracted mobilities, if overestimated, will be so by a similar amount, thus allowing an accurate comparison of the carrier mobilities of the different polymers relative to each other.

Because all polymers have identical conjugated backbones and comparable molecular weights, the observed differences in carrier mobilities likely originate from morphological differences in the polymer films, caused by the varying side chains. Grazing-incidence X-ray diffraction (GIXD) experiments were performed to probe the polymer film morphology and texture. All recorded GIXD images are provided in the Supporting Information (**Figure S13**), and the key

parameters extracted are presented in Table 2. The π-π stacking distances (~3.50 Å) of all polymers are not significantly affected by the different side chains, in contrast to the lamella stacking distances. The *d*-spacing is directly proportional to the alkyl chain length and increases gradually from 20.7 Å for **C₆C₁₀DPPT-TT** to 25.08 Å for **C₁₄C₁₀DPPT-TT** as shown in **Figure 4a**. The similar full width at half maximum (FWHM) values measured for the (100) diffraction peaks of all polymers, except **C₁₄C₁₀DPPT-TT**, indicates that the coherence lengths in the polymer crystallites is not significantly affected by the different side chain lengths, in contrast to the polymer chain orientation relative the substrate. Whereas the polymers with the shorter 4-hexyltetradecyl side chains adopt a nearly exclusive edge-on orientation, only 15% of the **C₁₄C₁₀DPPT-TT** polymer do so; in other words, the polymer chains prefer a face-on orientation (**Figure 4b**). In light of these results, the drop in hole mobility observed for **C₁₄C₁₀DPPT-TT** seems to be not so much the result of the long alkyl side chains, but rather as a consequence of the face-on orientation they assume. Interestingly, the highest hole mobilities were measured for **C₁₂C₁₀DPPT-TT**, which adopts only a partially face-on (58%) orientation. Mei *et al.* previously posited the idea of the formation of three-dimensional conduction channels in the presence of both edge-on and face-on domains in a polymer film.[31] It is noteworthy that the proposed three-dimensional conduction channels do not necessarily propagate throughout the bulk of the semiconducting film, considering that the charge carrier transport in OFET devices primarily occurs in the first layers of the semiconductor at the dielectric interface. However, the presence of such three-dimensional conducting pathways is thought to be beneficial for charge transport, as they allow charges to travel both in the planes perpendicular and parallel to the substrate, facilitating three-dimensional transport in the thin film and allowing the circumvention of defects and areas of low charge carrier mobility (e.g. grain boundaries, backbone torsional defects, etc.).

If the possibility of three-dimensional charge transport is a key requirement to achieve high carrier mobilities in organic semiconductors, it should be possible to induce such favorable morphology by blending different **C_xC_{10}DPPT-TT** polymers and thereby increasing the carrier mobility compared to the neat polymers. The GIXD studies revealed the different morphologies of each of the **C_xC_{10}DPPT-TT** polymers, and we therefore anticipate that by blending **C_6C_{10}DPPT-TT** (100% edge-on) with **$C_{14}C_{10}$DPPT-TT** (15% edge-on), it will be possible to mimic the favourable morphology of the **$C_{12}C_{10}$DPPT-TT** polymer. This hypothesis however underlies the assumption that the orientation behaviour of each polymer is unique and will not be significantly altered by blending with another polymer that is structurally similar.

To test this, both polymers (**C_6C_{10}DPPT-TT** and **$C_{14}C_{10}$DPPT-TT**) were blended (7:3 w/w, additional blends are summarized in Table S1), and the extracted field effect mobilities are depicted in **Figure 5** and summarized in the Supporting Information. The 7:3 blend ratio was chosen to adequately mimic a mixed morphology of edge-on and face-on orientations, whilst keeping the ratio of added polymer (**$C_{14}C_{10}$DPPT-TT** in this case) low to prevent significant phase separation. In an initial attempt, the OFET devices were annealed at 200°C given that these conditions were found to result in the best performing devices for the neat **C_xC_{10}DPPT-TT** polymers. However, in case of the polymer blend of **C_6C_{10}DPPT-TT** and **$C_{14}C_{10}$DPPT-TT**, we were not able to obtain similarly high performing devices and instead obtained hole mobilities comparable to the neat **$C_{14}C_{10}$DPPT-TT**-based devices. Even though the molecular structures of both polymers in the blend strongly resemble each other, it cannot be ruled out that the extended thermal annealing at elevated temperature leads to phase separation of both polymers. To verify this hypothesis, we lowered the annealing temperature to 150°C and shortened the annealing time (20 min) in order to allow residual solvent to evaporate from the film while at the same time reducing any possible phase separation. Indeed, the milder conditions improved the hole mobility from 1.5 $cm^2.V^{-1}.s^{-1}$ to 2.7 $cm^2.V^{-1}.s^{-1}$ for the blended

11

polymer device. Most interestingly though, the device with the blended semiconducting layer outperformed both the neat **C₆C₁₀DPPT-TT** and **C₁₄C₁₀DPPT-TT**, as well as the **C₁₂C₁₀DPPT-TT** when annealed at 150°C for a short time. Furthermore, GIXD measurements of the blended polymer film revealed a more complex film morphology (82% edge-on) than the two neat parent polymers **C₆C₁₀DPPT-TT** and **C₁₄C₁₀DPPT-TT**. Even though we were not able to exactly mimic the packing motif of the **C₁₂C₁₀DPPT-TT** polymer, our results strongly suggest that a mixed morphology of edge-on and face-on orientations in semiconducting polymer films is favourable for charge transport, in strong support of the existence of active, three-dimensional conduction channels during charge transport.

Encouraged by the results obtained with the blended polymer layer, we investigated if the mobility could be further improved by minimising phase separation within the polymer film. A random co-polymer (**RCP**) incorporating 70 mol% of monomer **10-a** and 30 mol% of **DPP** monomer **10-e** and 2,5-bis(trimethylstannyl)thieno[3,2-*b*]thiophene as the co-monomer was synthesised. The chemical structure is provided in the Supporting Information (Scheme S2), as well as all relevant characterization data. Whilst the DSC of the polymer blend (Figure S3) shows a broad endothermic transition at low temperature, resembling in width and shape the transitions observed for the individual polymers **C₆C₁₀DPPT-TT** and **C₁₄C₁₀DPPT-TT**, the RCP transition at low temperature is more subtle, comparable to the DSC trace of the neat **C₆C₁₀DPPT-TT** polymer. In OFET devices, the random co-polymer did outperform both parent co-polymer devices, **C₆C₁₀DPPT-TT** and **C₁₄C₁₀DPPT-TT**, as well as the corresponding polymer blend, when annealed at 200°C, but not the **C₁₂C₁₀DPPT-TT** device. At lower annealing temperatures (150°C), however, similar mobilities were measured for the **RCP** and **C₁₂C₁₀DPPT-TT**-based OFET devices, even though they were overall lower than for the blended polymer system. Intuitively, molecular packing behaviour similar to the blended polymer film might be expected for the **RCP** polymer, but the GIXD images (**Figure**

5b, bottom) revealed a nearly exclusive edge-on packing motif, comparable to **C₆C₁₀DPPT-TT**. This finding further supports the importance of three-dimensional conduction channels for optimizing charge carrier transport and, ultimately, mobility within semiconducting polymer films.

Besides the in-plane carrier mobilities measured in the OFETs, polymer chain orientation should also affect the out-of-plane charge transport. To probe any potential anisotropic charge transport, time-of-flight (ToF) measurements were performed on dropcast **C$_x$C₁₀DPPT-TT** polymer films. All polymers predominantly oriented edge-on relative to the substrate did not show any out-of-plane carrier mobilities and did display only featureless dispersive trapping. The trapping most likely results from the lack of adequate charge transport pathways along the lamella direction. Polymers **C₁₂C₁₀DPPT-TT** and **C₁₄C₁₀DPPT-TT**, as well as the blend of **C₆C₁₀DPPT-TT** and **C₁₄C₁₀DPPT-TT**, all of which show a stronger preference for partial face-on orientation, exhibited significantly less dispersive charge trapping. The out-of-plane hole mobilities are shown in **Figure 6** and summarized in the Supporting Information (Table S3). The inflection point was used to determine the arrival time t_0 instead of the time to one half-plateau height due to the dispersive nature exhibited in all of the samples. The hole mobility μ was calculated from the arrival time at a given bias V using the relationship

$$\mu = \frac{d^2}{Vt_0} \tag{1}$$

where d is the device thickness (~1 μm). In combination with the in-plane OFET mobility measurements, we believe that these results for the first time show strong experimental evidence in support of the three-dimensional conduction channel hypothesis stipulated in earlier works.

3. Conclusion

To study the influence of branched side chain geometries on charge carrier mobilities in DPP-based polymers, we synthesized a series of highly soluble **DPPT-TT** low-bandgap polymers with different branched alkyl side chains. Whereas the effects on optical properties were minor, GIXD experiments and OFET mobility measurements revealed significant differences among the various polymers. Whereas the polymers with the shorter branched side chains preferentially adopt an edge-on orientation on the substrate, longer branched alkyl chains induce a face-on orientation. This distinctive packing behaviour was found to lead to differences in charge carrier mobilities ranging from 1.4 to 3.7 $cm^2.V^{-1}.s^{-1}$. By blending polymers with different packing motifs, we were able to mimic the morphology of the polymer with the highest field effect mobilities. These findings unambiguously assert that a mixture of both edge-on and face-on polymer backbone orientations are highly beneficial for OFET device performance, most likely due to the formation of three-dimensional conduction channels. These pathways facilitate charge transport within the transistor channel by opening up alternative transport routes and allowing the carriers to bypass regions of low mobility (e.g. grain boundaries, poor orbital overlap, impurities, etc.).

Supporting Information

Supporting Information is available from the Wiley Online Library and includes detailed synthetic procedures, 1H- & 13C-NMR, UV-vis. spectra, cyclic voltammograms, TGA data, additional DSC curves, AFM and GIXD images, as well as transfer and output characteristics of all OFET devices are provided.

Received: ((will be filled in by the editorial staff))
Revised: ((will be filled in by the editorial staff))
Published online: ((will be filled in by the editorial staff))

References

[1]   H. Klauk, *Chemical Society Reviews* **2010**, 39, 2643.

[2]   a) T. Lei, J.-Y. Wang, J. Pei, *Chemistry of Materials* **2014**, 26, 594; b) J. Mei, Z. Bao, *Chemistry of Materials* **2014**, 26, 604.

[3]   a) A. Babel, S. A. Jenekhe, *Synthetic Metals* **2005**, 148, 169; b) B. C. Schroeder, S. Rossbauer, R. J. Kline, L. Biniek, S. E. Watkins, T. D. Anthopoulos, I. McCulloch, C. B. Nielsen, *Macromolecules* **2014**, 47, 2883; c) F. Hinkel, T. Marszalek, W. Zajaczkowski, S. R. Puniredd, M. Baumgarten, W. Pisula, K. Müllen, *Chemistry of Materials* **2014**, 26, 4844; d) I. Kang, H.-J. Yun, D. S. Chung, S.-K. Kwon, Y.-H. Kim, *Journal of the American Chemical Society* **2013**, 135, 14896; e) J. Y. Back, H. Yu, I. Song, I. Kang, H. Ahn, T. J. Shin, S.-K. Kwon, J. H. Oh, Y.-H. Kim, *Chemistry of Materials* **2015**, 27, 1732.

[4]   a) J. Lee, J. W. Chung, J. Jang, D. H. Kim, J.-I. Park, E. Lee, B.-L. Lee, J.-Y. Kim, J. Y. Jung, J. S. Park, B. Koo, Y. W. Jin, D. H. Kim, *Chemistry of Materials* **2013**, 25, 1927; b) Z. Fei, P. Pattanasattayavong, Y. Han, B. C. Schroeder, F. Yan, R. J. Kline, T. D. Anthopoulos, M. Heeney, *Journal of the American Chemical Society* **2014**, 136, 15154; c) B. Fu, J. Baltazar, A. R. Sankar, P.-H. Chu, S. Zhang, D. M. Collard, E. Reichmanis, *Advanced Functional Materials* **2014**, 24, 3734.

[5]   a) Y. W. Soon, S. Shoaee, R. S. Ashraf, H. Bronstein, B. C. Schroeder, W. Zhang, Z. Fei, M. Heeney, I. McCulloch, J. R. Durrant, *Advanced Functional Materials* **2014**, 24, 1474; b) T. Kurosawa, Y.-C. Chiu, Y. Zhou, X. Gu, W.-C. Chen, Z. Bao, *Advanced Functional Materials* **2016**, 26, 1261.

[6]   S. Savagatrup, A. S. Makaram, D. J. Burke, D. J. Lipomi, *Advanced Functional Materials* **2014**, 24, 1169.

[7]   a) L. Biniek, S. Fall, C. L. Chochos, D. V. Anokhin, D. A. Ivanov, N. Leclerc, P. Lévêque, T. Heiser, *Macromolecules* **2010**, 43, 9779; b) L. Ye, S. Zhang, L. Huo, M. Zhang, J. Hou, *Accounts of Chemical Research* **2014**, 47, 1595.

[8]   a) X. Zhang, L. J. Richter, D. M. DeLongchamp, R. J. Kline, M. R. Hammond, I. McCulloch, M. Heeney, R. S. Ashraf, J. N. Smith, T. D. Anthopoulos, B. Schroeder, Y. H. Geerts, D. A. Fischer, M. F. Toney, *Journal of the American Chemical Society* **2011**, 133, 15073; b) S. Fabiano, H. Yoshida, Z. Chen, A. Facchetti, M. A. Loi, *ACS Applied Materials & Interfaces* **2013**, 5, 4417; c) M. S. Chen, J. R. Niskala, D. A. Unruh, C. K. Chu, O. P. Lee, J. M. J. Fréchet, *Chemistry of Materials* **2013**, 25, 4088;

d) A. R. Han, J. Lee, H. R. Lee, J. Lee, S.-H. Kang, H. Ahn, T. J. Shin, J. H. Oh, C. Yang, *Macromolecules* **2016**, 49, 3739.

[9]   H. Sirringhaus, P. J. Brown, R. H. Friend, M. M. Nielsen, K. Bechgaard, B. M. W. Langeveld-Voss, A. J. H. Spiering, R. A. J. Janssen, E. W. Meijer, P. Herwig, D. M. de Leeuw, *Nature* **1999**, 401, 685.

[10]   a) Z. Bao, A. Dodabalapur, A. J. Lovinger, *Applied Physics Letters* **1996**, 69, 4108; b) B. S. Ong, Y. Wu, P. Liu, S. Gardner, *Journal of the American Chemical Society* **2004**, 126, 3378; c) I. McCulloch, M. Heeney, C. Bailey, K. Genevicius, I. MacDonald, M. Shkunov, D. Sparrowe, S. Tierney, R. Wagner, W. Zhang, M. L. Chabinyc, R. J. Kline, M. D. McGehee, M. F. Toney, *Nat Mater* **2006**, 5, 328; d) D. M. DeLongchamp, R. J. Kline, E. K. Lin, D. A. Fischer, L. J. Richter, L. A. Lucas, M. Heeney, I. McCulloch, J. E. Northrup, *Advanced Materials* **2007**, 19, 833; e) M. L. Chabinyc, M. F. Toney, R. J. Kline, I. McCulloch, M. Heeney, *Journal of the American Chemical Society* **2007**, 129, 3226.

[11]   I. Botiz, N. Stingelin, *Materials* **2014**, 7, 2273.

[12]   a) J. Mei, Y. Diao, A. L. Appleton, L. Fang, Z. Bao, *J Am Chem Soc* **2013**, 135, 6724; b) S. Holliday, J. E. Donaghey, I. McCulloch, *Chemistry of Materials* **2014**, 26, 647.

[13]   a) X. Zhang, H. Bronstein, A. J. Kronemeijer, J. Smith, Y. Kim, R. J. Kline, L. J. Richter, T. D. Anthopoulos, H. Sirringhaus, K. Song, M. Heeney, W. Zhang, I. McCulloch, D. M. DeLongchamp, *Nat Commun* **2013**, 4; b) D. Venkateshvaran, M. Nikolka, A. Sadhanala, V. Lemaur, M. Zelazny, M. Kepa, M. Hurhangee, A. J. Kronemeijer, V. Pecunia, I. Nasrallah, I. Romanov, K. Broch, I. McCulloch, D. Emin, Y. Olivier, J. Cornil, D. Beljonne, H. Sirringhaus, *Nature* **2014**, 515, 384.

[14]   R. Noriega, J. Rivnay, K. Vandewal, F. P. V. Koch, N. Stingelin, P. Smith, M. F. Toney, A. Salleo, *Nat Mater* **2013**, 12, 1038.

[15]   a) Y. Li, P. Sonar, L. Murphy, W. Hong, *Energy & Environmental Science* **2013**, 6, 1684; b) C. B. Nielsen, M. Turbiez, I. McCulloch, *Advanced Materials* **2013**, 25, 1859.

[16]   J. Liu, B. Walker, A. Tamayo, Y. Zhang, T.-Q. Nguyen, *Advanced Functional Materials* **2013**, 23, 47.

[17]   Z. Chen, M. J. Lee, R. Shahid Ashraf, Y. Gu, S. Albert-Seifried, M. Meedom Nielsen, B. Schroeder, T. D. Anthopoulos, M. Heeney, I. McCulloch, H. Sirringhaus, *Advanced Materials* **2012**, 24, 647.

[18]   Y. Diao, L. Shaw, Z. Bao, S. C. B. Mannsfeld, *Energy Environ. Sci.* **2014**, 7, 2145.

[19]   a) T. Lei, J.-H. Dou, J. Pei, *Advanced Materials* **2012**, 24, 6457; b) J. Lee, A. R. Han, H. Yu, T. J. Shin, C. Yang, J. H. Oh, *J Am Chem Soc* **2013**, 135, 9540; c) I. Meager, R. S. Ashraf, S. Mollinger, B. C. Schroeder, H. Bronstein, D. Beatrup, M. S. Vezie, T. Kirchartz, A. Salleo, J. Nelson, I. McCulloch, *Journal of the American Chemical Society* **2013**, 135, 11537; d) F. Zhang, Y. Hu, T. Schuettfort, C.-a. Di, X. Gao, C. R. McNeill, L. Thomsen, S. C. B. Mannsfeld, W. Yuan, H. Sirringhaus, D. Zhu, *Journal of the American Chemical Society* **2013**, 135, 2338.

[20]   J. Pei, T. Lei, J. Dou *Patent EP 2 698 835 A1*, **2014**.

[21]   B. Scheiper, M. Bonnekessel, H. Krause, A. Fürstner, *The Journal of Organic Chemistry* **2004**, 69, 3943.

[22]   a) F. C. Krebs, R. B. Nyberg, M. Jørgensen, *Chemistry of Materials* **2004**, 16, 1313; b) P. A. Troshin, D. K. Susarova, Y. L. Moskvin, I. E. Kuznetsov, S. A. Ponomarenko, E. N. Myshkovskaya, K. A. Zakharcheva, A. A. Balakai, S. D. Babenko, V. F. Razumov, *Advanced Functional Materials* **2010**, 20, 4351; c) J. K. Park, J. Jo, J. H. Seo, J. S. Moon, Y. D. Park, K. Lee, A. J. Heeger, G. C. Bazan, *Adv Mater* **2011**, 23, 2430; d) S. Kim, J. K. Park, Y. D. Park, *RSC Advances* **2014**, 4,

WILEY-VCH

39268; e) Ö. Usluer, M. Abbas, G. Wantz, L. Vignau, L. Hirsch, E. Grana, C. Brochon, E. Cloutet, G. Hadziioannou, *ACS Macro Letters* **2014**, 3, 1134.

[23] K. T. Nielsen, K. Bechgaard, F. C. Krebs, *Macromolecules* **2005**, 38, 658.

[24] H. Bronstein, Z. Chen, R. S. Ashraf, W. Zhang, J. Du, J. R. Durrant, P. Shakya Tuladhar, K. Song, S. E. Watkins, Y. Geerts, M. M. Wienk, R. A. J. Janssen, T. Anthopoulos, H. Sirringhaus, M. Heeney, I. McCulloch, *Journal of the American Chemical Society* **2011**, 133, 3272.

[25] H. Wu, B. Zhao, W. Wang, Z. Guo, W. Wei, Z. An, C. Gao, H. Chen, B. Xiao, Y. Xie, H. Wu, Y. Cao, *Journal of Materials Chemistry A* **2015**, 3, 18115.

[26] B. C. Schroeder, Y.-C. Chiu, X. Gu, Y. Zhou, J. Xu, J. Lopez, C. Lu, M. F. Toney, Z. Bao, *Advanced Electronic Materials* **2016**, 2, 1600104.

[27] J. Li, Y. Zhao, H. S. Tan, Y. Guo, C.-A. Di, G. Yu, Y. Liu, M. Lin, S. H. Lim, Y. Zhou, H. Su, B. S. Ong, *Scientific Reports* **2012**, 2, 754.

[28] a) D. Braga, G. Horowitz, *Advanced Materials* **2009**, 21, 1473; b) H. Sirringhaus, *Advanced Materials* **2014**, 26, 1319.

[29] I. McCulloch, A. Salleo, M. Chabinyc, *Science* **2016**, 352, 1521.

[30] T. Uemura, C. Rolin, T.-H. Ke, P. Fesenko, J. Genoe, P. Heremans, J. Takeya, *Advanced Materials* **2016**, 28, 151.

[31] J. Mei, D. H. Kim, A. L. Ayzner, M. F. Toney, Z. Bao, *Journal of the American Chemical Society* **2011**, 133, 20130.
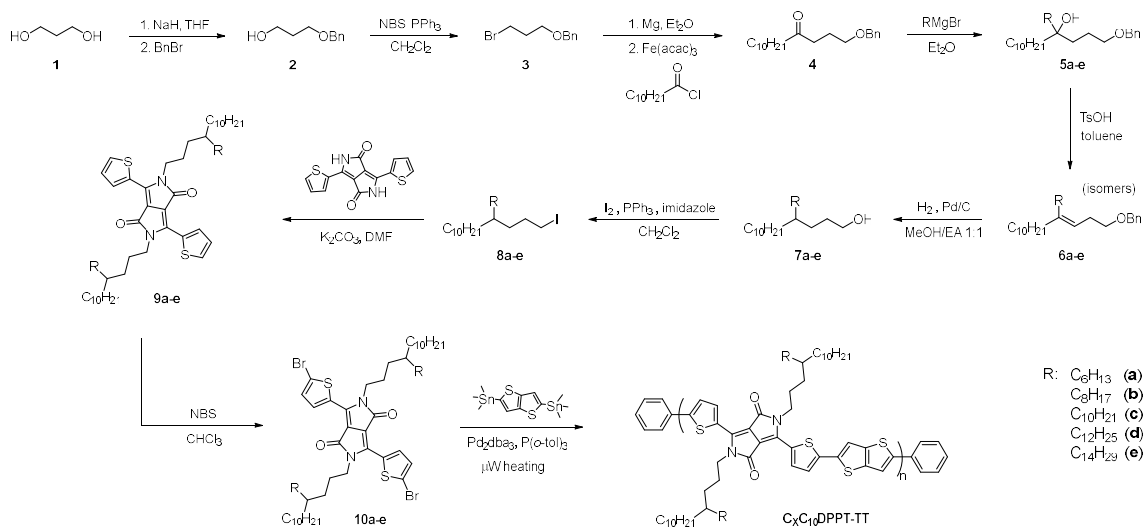
Scheme 1. Synthetic pathway towards the different **CxC₁₀DPPT-TT** polymers.

Table 1. Molecular weights of the different **C$_x$C$_{10}$DPPT-TT**.

Polymer	M$_n$ [a) [kg.mol^{-1}]	M$_w$ [b) [kg.mol^{-1}]	Đ$_w$ [c)	DP$_n$ [d)
C$_6$C$_{10}$DPPT-TT	45	139	3.1	45
C$_8$C$_{10}$DPPT-TT	49	155	3.2	46
C$_{10}$C$_{10}$DPPT-TT	53	163	3.1	47
C$_{12}$C$_{10}$DPPT-TT	51	162	3.2	44
C$_{14}$C$_{10}$DPPT-TT	53	149	2.8	43

[a) Number-average molecular weight. [b) Weight-average molecular weight. [c) Weight dispersity defined as M$_w$/M$_n$. [d) Number-average degree of polymerization.
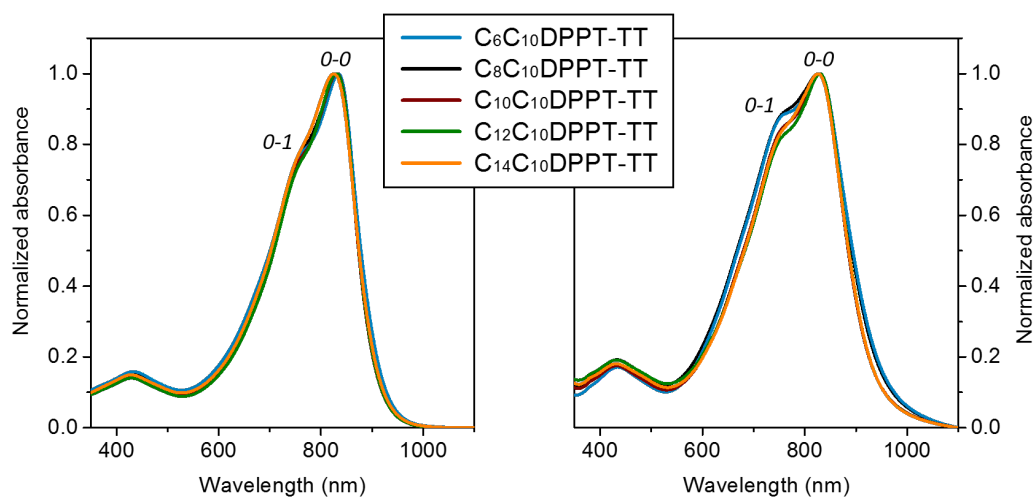
Figure 1. UV-*vis.* absorption spectra of all **C$_x$C$_{10}$DPPT-TT** polymers in dilute chlorobenzene solution (left) and in thin film (right) spin-coated at a concentration of 5 mg.mL^{-1}.
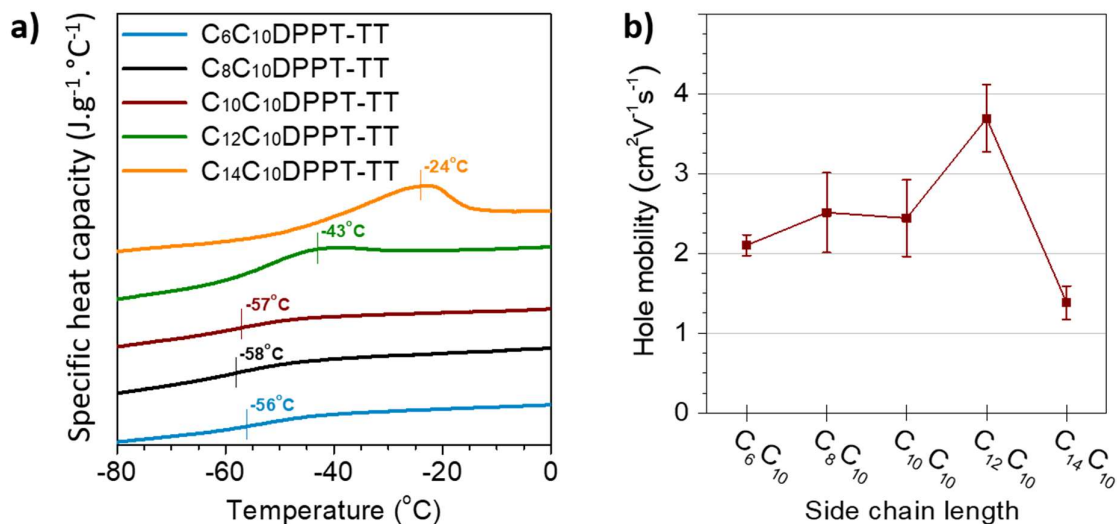
Figure 2. (a) DSC traces of **CₓC₁₀DPPT-TT** polymers during the second heating cycle (endo up) recorded at a heating rate of 10°C.min^{-1}. (b) Hole mobilities (averaged over 10 devices) of the different **CₓC₁₀DPPT-TT** polymers measured in bottom-gate, top-contact OFET devices plotted against the alkyl side chain length.
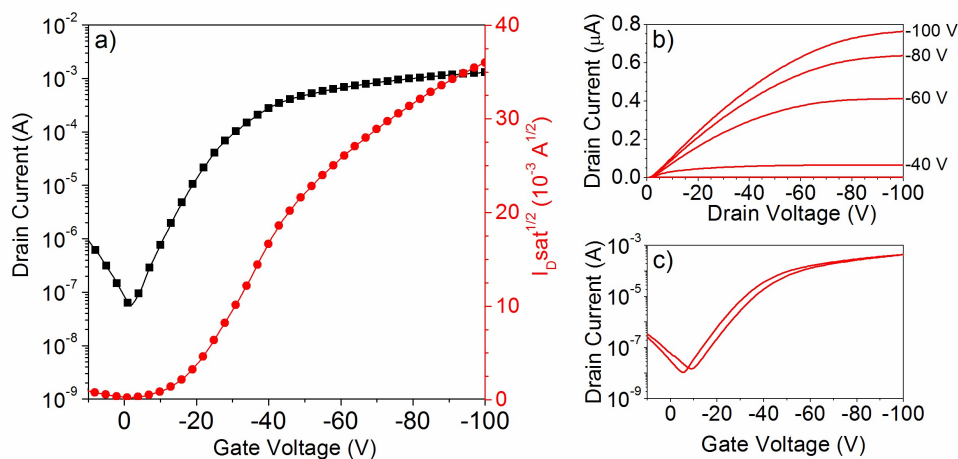

Figure 3. (a) Transfer curve, (b) output characteristics and (c) hysteresis of a BGTC OFET device using the **C₁₂C₁₀DPPT-TT** polymer as active material after thermal annealing at 200°C during 1 hour.

Table 2. Crystallographic parameters for $C_xC_{10}DPPT-TT$ polymers after annealing for 1 hour at 200°C.

Polymer	Lamellar spacing [a] [Å]	Lamellar peak FWHM [Å^{-1}]	π-π spacing [b] [Å]	π-π peak FWHM [Å^{-1}]
$C_6C_{10}DPPT-TT$	20.7	0.032	3.6	0.063
$C_8C_{10}DPPT-TT$	21.9	0.031	3.6	0.062
$C_{10}C_{10}DPPT-TT$	23.1	0.031	3.5	0.095
$C_{12}C_{10}DPPT-TT$	24.1	0.032	3.5	0.093
$C_{14}C_{10}DPPT-TT$	25.1	0.038	3.5	0.080
blend	22.5	0.037	3.6	0.077
RCP	21.8	0.032	3.6	0.067

[a] Obtained from fitting the (200) diffraction peak. [b] Extracted by fitting the (010) diffraction peak.
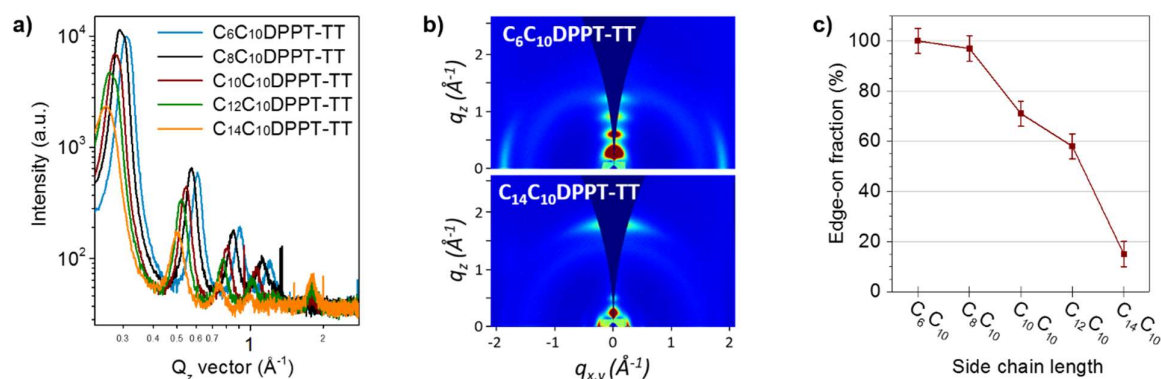
Figure 4. (a) The diffraction intensity in the out of the plane direction plotted against the approximate scattering vector of **$C_xC_{10}DPPT-TT$** polymer along the meridian. (b) GIXD diffraction patterns of **$C_6C_{10}DPPT-TT$** (top) and **$C_{14}C_{10}DPPT-TT$** (bottom). (c) The edge-on fraction of the polymer film as a function of side chain lengths. Details on how the edge-on fraction was calculated can be found in the Supporting Information.
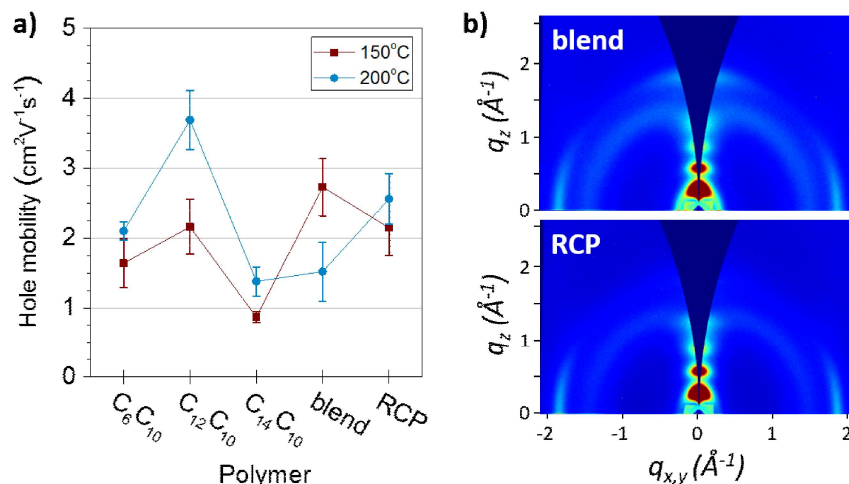
Figure 5. (a) Hole mobilities (averaged over 10 devices) of the different **C$_x$C$_{10}$DPPT-TT** polymers and blend measured in bottom-gate, top-contact OFET. The lines between experimental data points were added to guide the eye. (b) GIXD diffraction patterns of the **C$_6$C$_{10}$DPPT-TT:C$_{14}$C$_{10}$DPPT-TT** blend (7:3) (top) and the corresponding random co-polymer (RCP) (bottom).
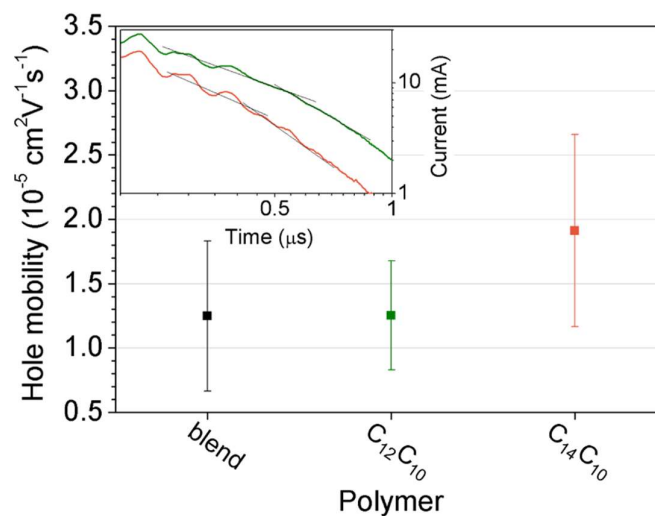
Figure 6. Calculated hole mobilities for the polymers **C$_{12}$C$_{10}$DPPT-TT**, **C$_{14}$C$_{10}$DPPT-TT** and the polymer blend. The insert shows the transient photocurrents and the arrival times for the same (unblended) polymers at an applied bias of +20V.

The solid state packing and morphology of semiconducting polymers play a key role in achieving high charge carrier mobilities in field effect transistors. In this work, the creation of three-dimensional transport pathways in organic semiconductors is found to be beneficial for charge transport, and can be artificially engineered by blending polymers with different solid state packing motifs.

Bob C. Schroeder, Tadanori Kurosawa, Tianren Fu, Yu-Cheng Chiu, Jaewan Mun, Ging-Ji Nathan Wang, Xiaodan Gu, Leo Shaw, James W. E. Kneller, Theo Kreouzis, Michael F. Toney and Zhenan Bao*

Taming charge transport in semiconducting polymers with branched alkyl side chains.

WILEY-VCH
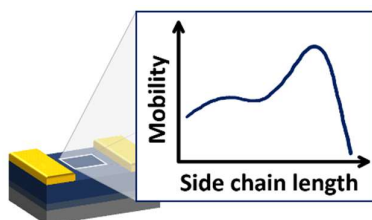
Supporting Information

Taming charge transport in semiconducting polymers with branched alkyl side chains.

Bob C. Schroeder, Tadanori Kurosawa, Tianren Fu, Yu-Cheng Chiu, Jaewan Mun, Ging-Ji Nathan Wang, Xiaodan Gu, Leo Shaw, James W. E. Kneller, Theo Kreouzis, Michael F. Toney, and Zhenan Bao*

Table of Contents

Synthetic methods and characterization

All reagents and solvents were obtained from commercial suppliers and used without further purification. The 3,6-di(thiophen-2-yl)-2,5-dihydropyrrolo[3,4-c]pyrrole-1,4-dione core (DPPT) was synthesized according to literature.[1] All polymerization reaction were conducted in a CEM Discover microwave reactor. Nuclear magnetic resonance (NMR) spectra were recorded on a 400 MHz Varian Mercury spectrometer at 293 K and referenced against the residual solvent peak. Polymer number-average (M_n) and weight-average (M_w) molecular weights were measured on a Tosoh high-temperature EcoSEC system, equipped with a TSKgel GPC column (GMHHR-H; 300 mm × 7.8 mm) at 200°C using 1,2,4-trichlorobenzene as eluent. Prior to the measurements, the system was calibrated against narrow weight-average dispersity (Đ < 1.10) polystyrene standards. Cyclic voltammetry measurements on polymer thin-films were performed using an CH Instrument potentiostat with a standard three-electrode setup. A glassy carbon electrode served as working electrode, a Ag/Ag$^+$ reference electrode calibrated against Fc/Fc$^+$ and a platinum rod as counter electrode. A 10 mg.mL^{-1} polymer solution in chlorobenzene was dropcasted onto a circular glassy carbon electrode. The solvent was evaporated under a gentle nitrogen stream. The measurements were carried out at room temperature in anhydrous and deoxygenated acetonitrile with 0.1 M tetrabutylammonium hexafluorophosphate as the supporting electrolyte at a scan rate of 50 mV.s^{-1}. UV-vis. absorption spectra in solution and thin film were recorded on an Agilent Cary 6000i UV/Vis/NIR spectrometer. Differential scanning calorimetry (DSC) experiments were performed with a TA Instruments DSC Q2000 using Tzero aluminum pans. Thermal stability measurements were conducted with Mettler Toledo AG-TGA/SDTA851e. Polymer grazing-incidence X-ray diffraction (GIXD) measurements were performed at the Stanford Synchrotron Radiation Lightsource on beamline 11-3 with a photon energy of 12.73 keV. The angle of incidence was fixed at 0.12° to enhance the diffraction intensity and probe the entire thickness of the films.
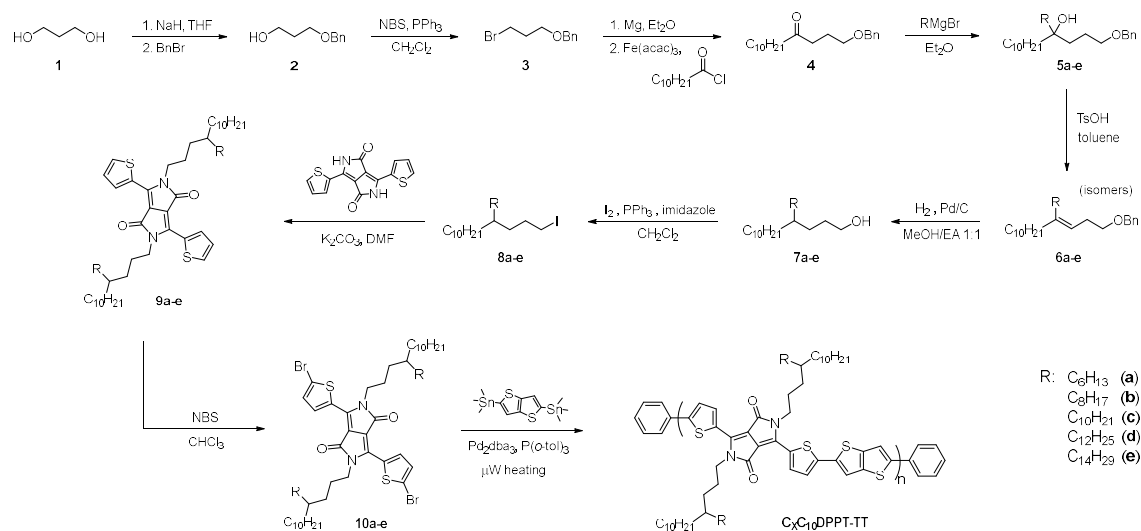
Scheme S1. Synthetic pathway towards the various **C$_x$C$_{10}$DPPT-TT** polymers.

3-(benzyloxy)propan-1-ol (2)

14 g of sodium hydride dispersed in mineral oil (60% wt.) were introduced into a 1L two-necked round bottom flask. 150 mL of anhydrous hexane were added and the suspension stirred during 5 minutes under nitrogen atmosphere. The hexane was decanted, whilst maintaining a constant flow of nitrogen over the washed sodium hydride. The procedure was repeated two more times, before the washed sodium hydride (8.7g, 361 mmol) was dried under vacuum for 2 hours. The dried sodium hydride was suspended in a mixture of 400 mL anhydrous THF and 100 mL anhydrous DMF and then cooled down to 0°C. propane-1,3-diol (23.6 mL, 329 mmol) was added slowly to the sodium hydride suspension. After complete addition the reaction mixture is allowed to warm to room temperature and stirred for 3 hours. Benzyl bromide (42.9 mL, 361 mmol) was diluted in 40 mL of anhydrous THF and added slowly to the reaction mixture at 0°C. After complete addition the reaction mixture is slowly heated to reflux and maintained at that temperature overnight. The reaction is cooled to room temperature and carefully quenched by addition of water. The mixture is diluted with ethyl acetate (300 mL), and the organic phase is separated. The organic layer is washed with water (2×200 mL) and brine (1×200 mL) and finally dried over $MgSO_4$. After solvent evaporation, the crude product is purified by distillation under reduced pressure and the title compound recovered as a colorless oil (32.8 g, 197 mmol, 60%). ^{1}H NMR (400 MHz, $CDCl_3$) δ 7.42 – 7.19 (m, 5H), 4.50 (s, 2H), 3.57 (t, $J = 6.1$ Hz, 2H), 3.50 (t, $J = 6.0$ Hz, 2H), 1.73 – 1.58 (m, 2H). ^{13}C NMR (100 MHz, $CDCl_3$) δ 138.09, 128.28, 127.59, 127.52, 72.83, 70.19, 62.15, 29.66, 26.35.

((3-bromopropoxy)methyl)benzene (3)

3-(benzyloxy)propan-1-ol (30.0 g, 181 mmol) (2) and triphenylphosphine (56.8 g, 217 mmol) were dissolved in 300 mL of dichloromethane and cooled to 0°C. *N*-bromosuccinimide (38.5 g, 217 mmol) was added in several portions over the course of 30 minutes, and the reaction allowed to stir overnight at room temperature. The reaction mixture was added to water (300 mL), and the organic layer separated and washed with water (2×200 mL) and brine (1×200 mL) and dried over $MgSO_4$ before being concentrated on a rotary evaporator. The concentrated solution was added to vigorously stirred hexane (300 mL) in order to precipitate most of the triphenylphosphine oxide formed during the reaction. The white precipitate was filtered off and the hexane evaporated. The recovered orange oil was further purified by distillation under reduced pressure to recover ((3-bromopropoxy)methyl)benzene as a colourless oil (38.3 g, 167 mmol, 93%). ^{1}H NMR (400 MHz, $CDCl_3$) δ 7.35 – 7.23 (m, 5H), 4.48 (s, 2H), 3.56 (t, $J = 5.8$ Hz, 2H), 3.49 (t, $J = 6.6$ Hz, 2H), 2.15 – 2.05 (m, 2H). ^{13}C NMR (100 MHz, $CDCl_3$) δ 138.28, 128.45, 127.70, 127.68, 73.14, 67.72, 32.95, 30.75.

1-(benzyloxy)pentadecan-4-one (4) [2]

Magnesium turnings (1.7 g, 71.5 mmol) in anhydrous THF (20 mL) were activated by adding three times 5 drops of 1,2-dibromoethane and stirring at reflux temperature for 2 minutes. After the activation was confirmed by the generation of ethylene gas, ((3-bromopropoxy)methyl)benzene (14.9 g, 65.0 mmol) (3) diluted in anhydrous THF (15 mL) was added dropwise and the Grignard reagent was prepared at reflux temperature in 1 hour. Meanwhile, a solution of undecanoyl chloride (15.7 mL, 71.5 mmol) and iron(III) acetylacetonate (0.76 g, 2.2 mmol) in dry THF was cooled to –78°C using a dry ice and acetone bath. To this solution was added the above Grignard solution dropwise, and the reaction mixture was stirred for 1 h at the same temperature. After quenching the reaction using saturated NH_4Cl aqueous solution, the mixture was warmed up to room temperature and extracted with ethyl acetate. The solvent was removed under reduced pressure after drying over

Na$_2$SO$_4$, and the crude compound was purified by column chromatography (silica gel: 500 mL; eluent: hexane/ ethyl acetate = 100/1 for 2 column volumes, 50/1 for 2 column volumes, and 30/1 until all the ketone was recovered) to obtain 13.1 g (63%) of the desired compound as a colorless oil. ^{1}H NMR (400 MHz, CDCl$_3$) δ 7.59 – 7.01 (m, 5H), 4.48 (s, 2H), 3.48 (t, J = 6.1 Hz, 2H), 2.52 (t, J = 7.2 Hz, 2H), 2.38 (t, J = 7.5 Hz, 2H), 1.94 – 1.82 (m, 2H), 1.59 – 1.47 (m, 2H), 1.29 – 1.21 (m, 14H), 0.88 (t, J = 6.8 Hz, 3H). ^{13}C NMR (100 MHz, CDCl$_3$) δ 211.27, 138.54, 128.51, 127.78, 127.71, 72.99, 69.51, 43.09, 39.43, 32.04, 29.72, 29.63, 29.57, 29.46, 29.40, 29.21, 24.01, 22.83, 14.27.

General procedure for the preparation of 1-(benzyloxy)-4-alkyltetradecan-4-ol (5a-e)

3.00 g (9.4 mmol) of 1-(benzyloxy)tetradecan-4-one is dissolved in 100 mL of anhydrous diethyl ether and cooled to 0°C. Afterwards, 1.1 equivalent of Grignard reagent in a 2 M diethyl ether solution is added dropwise. After complete addition, the reaction mixture is refluxed for 16 hours. After the reaction was cooled to room temperature, it was quenched into an ice-cooled aqueous ammonium chloride solution (10%). The aqueous phase was extracted three times with diethyl ether (100 mL). The combined organic layers were washed with brine and dried over sodium sulfate. After filtration the solvent was evaporated under reduced pressure to recover the crude product as yellow/orange oil. After column chromatography using a 5:1 hexanes:ethyl acetate eluent, the title compound was recovered as pale yellow/orange oil.

7-(3-(benzyloxy)propyl)heptadecan-7-ol (5a)

The title compound was recovered as pale orange oil (3.1 g, 7.6 mmol, 81%). ^{1}H NMR (400 MHz, CDCl$_3$) δ 7.30 – 7.18 (m, 5H), 4.44 (s, 2H), 3.41 (t, J = 6.3 Hz, 2H), 1.67 – 1.53 (m, 3H), 1.47 – 1.41 (m, 2H), 1.38 – 1.29 (m, 4H), 1.26 – 1.13 (m, 24H), 0.81 (t, J = 6.7 Hz, 6H). ^{13}C NMR (100 MHz, CDCl$_3$) δ 138.51, 128.49, 127.74, 127.67, 77.16, 74.09, 73.05, 71.12, 39.37, 36.23, 32.06, 32.01, 30.43, 30.10, 29.79, 29.78, 29.49, 24.05, 23.68, 23.65, 22.83, 22.80, 14.27, 14.25.

9-(3-(benzyloxy)propyl)nonadecan-9-ol (5b)

The title compound was recovered as pale yellow oil (3.6 g, 8.3 mmol, 88%). ^{1}H NMR (400 MHz, CDCl$_3$) δ 7.30 – 7.18 (m, 5H), 4.44 (s, 2H), 3.41 (t, J = 6.4 Hz, 2H), 1.69 – 1.52 (m, 3H), 1.46 – 1.40 (m, 2H), 1.38 – 1.30 (m, 4H), 1.26 – 1.13 (m, 28H), 0.81 (t, J = 6.8 Hz, 6H). ^{13}C NMR (100 MHz, CDCl$_3$) δ 138.52, 128.49, 127.75, 127.67, 74.10, 73.05, 71.13, 39.36, 36.24, 32.06, 32.04, 30.43, 29.79, 29.78, 29.75, 29.49, 29.46, 24.05, 23.69, 22.83, 22.82, 14.26.

11-(3-(benzyloxy)propyl)henicosan-11-ol (5c)

The title compound was recovered as colorless oil (3.5 g, 7.6 mmol, 81%). ^{1}H NMR (400 MHz, CDCl$_3$) δ 7.40 – 7.21 (m, 5H), 4.52 (s, 2H), 3.49 (t, J = 6.3 Hz, 2H), 1.71 (s, 1H), 1.69 – 1.62 (m, 2H), 1.54 – 1.48 (m, 2H), 1.46 – 1.39 (m, 4H), 1.32 – 1.24 (m, 32H), 0.89 (t, J = 6.9 Hz, 6H). ^{13}C NMR (100MHz, CDCl$_3$) δ 138.50, 128.47, 127.72, 127.64, 77.16, 74.05, 73.02, 71.11, 39.35, 36.22, 32.05, 30.42, 29.79, 29.77, 29.48, 24.04, 23.68, 22.82, 14.26.

11-(3-(benzyloxy)propyl)tricosan-11-ol (5d)

The title compound was recovered as pale yellow oil (3.6 g, 7.3 mmol, 78%). ^{1}H NMR (400 MHz, CDCl$_3$) δ 7.38 – 7.24 (m, 5H), 4.52 (s, 2H), 3.49 (t, J = 6.3 Hz, 2H), 1.74 (s, 1H), 1.71 – 1.61 (m, 2H), 1.55 – 1.48 (m, 2H), 1.46 – 1.38 (m, 4H), 1.32 – 1.24 (m, 36H), 0.89 (t, J = 6.8

Hz, 6H). ^{13}C NMR (100 MHz, CDCl$_3$) δ 138.49, 128.45, 127.70, 127.63, 74.03, 73.01, 71.09, 39.34, 36.21, 32.04, 30.42, 29.81, 29.78, 29.76, 29.49, 29.48, 24.02, 23.67, 22.81, 14.24.

11-(3-(benzyloxy)propyl)pentacosan-11-ol (5e)

The title compound was recovered as colorless oil (3.4 g, 7.0 mmol, 70%). ^{1}H NMR (400 MHz, CDCl$_3$) δ 7.29 – 7.18 (m, 5H), 4.44 (s, 2H), 3.41 (t, J = 6.3 Hz, 2H), 1.66 – 1.50 (m, 2H), 1.47 – 1.41 (m, 2H), 1.38 – 1.30 (m, 4H), 1.23 – 1.15 (m, 40H), 0.81 (t, J = 6.9 Hz, 6H). ^{13}C NMR (100 MHz, CDCl$_3$) δ 138.48, 128.48, 127.74, 127.66, 74.15, 73.03, 71.11, 39.33, 36.22, 32.07, 32.06, 30.43, 29.85, 29.83, 29.80, 29.51, 29.49, 24.03, 23.68, 22.83, 14.27.

General procedure for the hydroxyl group elimination (6a-e)

7 mmol of 1-(benzyloxy)-4-alkyltetradecan-4-ol (5a-e) are dissolved in 150 mL of toluene and 1 mol% of *p*-toluenesulfonic acid was added. The reaction mixture was refluxed for 12 hours in a Dean-Stark apparatus. Afterwards the cooled down mixture was washed with 100 mL of water, followed by 100 mL of brine. After drying over MgSO$_4$, the toluene solution was filtered-off and evaporated. A mixture of title compound isomers was recovered as a yellow to orange oil and used without further purification in the next step.

(((4-hexyltetradec-3-en-1-yl)oxy)methyl)benzene (6a)

The title compound was recovered as orange oil (2.6 g, 6.7 mmol, 96%). ^{1}H NMR (400 MHz, CDCl$_3$) δ 7.35 – 7.16 (m, 5H), 5.14 – 5.06 (m, 1H), 4.53 – 4.49 (m, 2H), 3.49 – 3.42 (m, 2H), 2.11 – 1.92 (m, 4H), 1.75 – 1.60 (m, 2H), 1.36 – 1.22 (m, 24H), 0.88 (t, J = 6.7 Hz, 6H). ^{13}C NMR (100 MHz, CDCl$_3$) δ 128.48, 127.78, 127.60 73.01, 70.47, 32.08, 29.80, 29.76, 29.63, 29.51, 28.66, 26.55, 22.84, 22.78, 14.28.

(((4-octyltetradec-3-en-1-yl)oxy)methyl)benzene (6b)

The title compound was recovered as pale orange oil (2.8 g, 6.7 mmol, 96%). ^{1}H NMR (400 MHz, CDCl$_3$) δ 7.40 – 7.18 (m, 5H), 5.16 – 5.04 (m, 1H), 4.54 – 4.48 (m, 2H), 3.51 – 3.42 (m, 2H), 2.13 – 1.91 (m, 4H), 1.77 – 1.48 (m, 2H), 1.38 – 1.18 (m, 28H), 0.89 (t, J = 6.7 Hz, 6H). ^{13}C NMR (100 MHz, CDCl$_3$) δ 128.47, 127.77, 127.60, 73.00, 70.46, 32.07, 29.81, 29.76, 29.51, 22.85, 14.28.

(((4-decyltetradec-3-en-1-yl)oxy)methyl)benzene (6c)

The title compound was recovered as pale yellow oil (2.9 g, 6.6 mmol, 94%). ^{1}H NMR (400 MHz, CDCl$_3$) δ 7.39 – 7.24 (m, 5H), 5.17 – 5.08 (m, 1H), 4.54 – 4.49 (m, 2H), 3.50 – 3.41 (m, 2H), 2.06 – 1.93 (m, 4H), 1.77 – 1.65 (m, 2H), 1.39 – 1.21 (m, 32H), 0.90 (t, J = 6.8 Hz, 6H). ^{13}C NMR (100 MHz, CDCl$_3$) δ 138.88, 128.57, 127.87, 127.85, 127.71, 125.49, 119.98, 73.11, 70.73, 70.44, 37.07, 33.49, 32.19, 30.42, 30.38, 30.26, 30.06, 29.93, 29.87, 29.74, 29.63, 28.77, 28.72, 28.52, 27.97, 26.64, 22.96, 14.39.

(((4-decylhexadec-3-en-1-yl)oxy)methyl)benzene (6d)

The title compound was recovered as yellow oil (3.2 g, 6.9 mmol, 98%). ^{1}H NMR (400 MHz, CDCl$_3$) δ 7.40 – 7.11 (m, 5H), 5.17 – 5.07 (m, 1H), 4.57 – 4.46 (m, 2H), 3.53 – 3.41 (m, 2H), 2.12 – 1.94 (m, 4H), 1.76 – 1.61 (m, 2H), 1.37 – 1.25 (m, 36H), 0.89 (t, J = 6.8 Hz, 6H). ^{13}C NMR (100 MHz, CDCl$_3$) δ 128.50, 127.75, 127.73, 127.59, 73.02, 70.63, 70.33, 32.08, 29.98, 29.81, 29.77, 29.53, 22.85, 14.28.

(((4-decyloctadec-3-en-1-yl)oxy)methyl)benzene (6e)

The title compound was recovered as yellow oil (3.5 g, 6.9 mmol, 99%). ^{1}H NMR (400 MHz, CDCl$_3$) δ 7.39 – 7.22 (m, 5H), 5.16 – 5.05 (m, 1H), 4.57 – 4.45 (m, 2H), 3.53 – 3.40 (m, 2H), 2.06 – 1.93 (m, 4H), 1.79 – 1.56 (m, 2H), 1.38 – 1.20 (m, 40H), 0.88 (t, J = 6.9 Hz, 6H). ^{13}C NMR (100 MHz, CDCl$_3$) δ 128.47, 127.77, 127.61, 73.00, 70.63, 70.34, 32.09, 29.86, 29.82, 29.77, 29.59, 29.53, 22.85, 14.29.

Preparation of 4-alkyltetradecan-1-ol (7a-e)

7 mmol of the corresponding alkene (6a-e) were dissolved in a 160 mL solution of methanol:ethyl acetate (1:1). 2 mol% of Pd/C (calculated by Pd content) were added. The reaction mixture was stirred during 24 hours under a 1 atm H$_2$ atmosphere at room temperature. Afterwards the reaction mixture was filtered through a Celite^{TM} plug using ethyl acetate as eluent. The crude product was recovered as colorless to pale yellow oil and used without further purification in the next step.

4-hexyltetradecan-1-ol (7a)

The title compound was recovered as yellow oil (1.8 g, 6.1 mmol, 87%). ^{1}H NMR (400 MHz, CDCl$_3$) δ 3.62 (t, J = 6.7 Hz, 2H), 1.64 – 1.48 (m, 3H), 1.40 (s, 1H), 1.32 – 1.17 (m, 30H), 0.87 (t, J = 6.6 Hz, 6H). ^{13}C NMR (100 MHz, CDCl$_3$) δ 63.72, 37.37, 33.73, 32.08, 30.28, 30.10, 29.95, 29.86, 29.81, 29.67, 29.52, 26.80, 26.77, 22.85, 14.27.

4-octyltetradecan-1-ol (7b)

The title compound was recovered as yellow oil (2.2 g, 6.8 mmol, 98%). ^{1}H NMR (400 MHz, CDCl$_3$) δ 3.62 (t, J = 6.7 Hz, 2H), 1.62 – 1.50 (m, 3H), 1.42 (s, 1H), 1.34 – 1.19 (m, 34H), 0.88 (t, J = 6.8 Hz, 6H). ^{13}C NMR (100 MHz, CDCl$_3$) δ 63.88, 37.37, 33.73, 32.08, 30.28, 29.86, 29.52, 26.80, 22.85, 14.28.

4-decyltetradecan-1-ol (7c)

The title compound was recovered as pale yellow oil (2.5 g, 6.9 mmol, 99%). ^{1}H NMR (400 MHz, CDCl$_3$) δ 3.62 (t, J = 5.7 Hz, 2H), 1.58 – 1.46 (m, 3H), 1.40 (s, 1H), 1.31 – 1.21 (m, 34H), 0.86 (t, J = 6.8 Hz, 6H). ^{13}C NMR (100 MHz, CDCl$_3$) δ 63.69, 37.36, 33.71, 32.09, 30.29, 30.08, 29.87, 29.83, 29.66, 29.54, 26.80, 22.85, 14.28.

4-decylhexadecan-1-ol (7d)

The title compound was recovered as yellow oil (2.7 g, 6.9 mmol, 99%). ^{1}H NMR (400 MHz, CDCl$_3$) δ 3.62 (t, J = 6.8 Hz, 2H), 1.61 – 1.49 (m, 3H), 1.42 (s, 1H), 1.30 – 1.21 (m, 42H), 0.88 (t, J = 6.8 Hz, 6H). ^{13}C NMR (100 MHz, CDCl$_3$) δ 63.72, 37.16, 33.72, 32.08, 30.28, 29.87, 29.82, 29.52, 26.80, 22.85, 14.29.

4-decyloctadecan-1-ol (7e)

The title compound was recovered as yellow oil (2.9 g, 6.9 mmol, 99%). ^{1}H NMR (400 MHz, CDCl$_3$) δ 3.62 (t, J = 6.7 Hz, 2H), 1.67 – 1.49 (m, 3H), 1.40 (s, 1H), 1.33 – 1.18 (m, 46H), 0.88 (t, J = 6.8 Hz, 6H). ^{13}C NMR (100 MHz, CDCl$_3$) δ 63.88, 37.16, 33.72, 32.08, 30.28, 29.86, 29.82, 29.52, 26.80, 22.85, 14.29.

Preparation of 4-alkyl-tetradecyl iodide (8a-e)

6 mmol of 4-alkyltetradecan-1-ol (7a-e) were dissolved in 100 mL of dichloromethane; 1.2 equivalents of triphenylphosphine and 1.5 equivalent of imidazole were added and the solution was cooled to 0 °C. Once cooled down, 1.3 equivalents of iodine were added, and the reaction was stirred for 3 hours. The reaction was quenched by addition of 50 mL of sodium sulfite. The organic layer was separated and washed with water (100 mL) followed by brine (100 mL). The solution was dried over $MgSO_4$ and the solvent evaporated. The crude product was filtered through a short silica plug using hexane as eluent and recovered as a colorless oil after solvent evaporation.

7-(3-iodopropyl)heptadecane (8a)

The title compound was recovered as colorless oil (1.9 g, 4.6 mmol, 77%). ^{1}H NMR (400 MHz, CDCl$_3$) δ 3.17 (t, J = 7.1 Hz, 2H), 1.86 – 1.72 (m, 2H), 1.36 – 1.17 (m, 31H), 0.92 – 0.84 (m, 6H). ^{13}C NMR (100 MHz, CDCl$_3$) δ 36.87, 34.70, 33.72, 33.71, 32.08, 31.08, 30.23, 29.91, 29.85, 29.82, 29.53, 26.78, 26.76, 22.88, 22.86, 14.29.

9-(3-iodopropyl)nonadecane (8b)

The title compound was recovered as colorless oil (1.9 g, 4.3 mmol, 72%). ^{1}H NMR (400 MHz, CDCl$_3$) δ 3.17 (t, J = 7.1 Hz, 2H), 1.84 – 1.74 (m, 2H), 1.46 – 1.17 (m, 35H), 0.88 (t, J = 6.8 Hz, 6H). ^{13}C NMR (100 MHz, CDCl$_3$) δ 36.85, 34.69, 33.70, 32.08, 31.07, 30.24, 29.86, 29.82, 29.53, 26.78, 22.86, 14.29, 7.92.

11-(3-iodopropyl)henicosane (8c)

The title compound was recovered as colorless oil (2.6 g, 5.5 mmol, 92%). ^{1}H NMR (400 MHz, CDCl$_3$) δ 3.17 (t, J = 7.1 Hz, 2H), 1.85 – 1.75 (m, 2H), 1.39 – 1.17 (m, 39H), 0.88 (t, J = 6.7 Hz, 6H). ^{13}C NMR (100 MHz, CDCl$_3$) δ 36.84, 34.68, 33.68, 32.09, 32.07, 31.06, 30.23, 29.85, 29.82, 29.81, 29.53, 26.77, 22.86, 14.30.

11-(3-iodopropyl)tricosane (8d)

The title compound was recovered as colorless oil (2.5 g, 5.1 mmol, 85%). ^{1}H NMR (400 MHz, CDCl$_3$) δ 3.16 (t, J = 7.1 Hz, 2H), 1.83 – 1.75 (m, 2H), 1.37 – 1.19 (m, 43H), 0.89 (t, J = 6.9 Hz, 6H). ^{13}C NMR (100 MHz, CDCl$_3$) δ 36.84, 34.68, 33.97, 33.70, 32.07, 31.06, 30.23, 30.20, 29.80, 29.77, 29.66, 29.51, 26.78, 22.84, 14.28.

11-(3-iodopropyl)pentacosane (8e)

The title compound was recovered as colorless oil (2.6 g, 5.0 mmol, 83%). ^{1}H NMR (400 MHz, CDCl$_3$) δ 3.17 (t, J = 7.1 Hz 2H), 1.85 – 1.75 (m, 2H), 1.19 – 1.21 (m, 47H), 0.89 (t, J = 6.9 Hz, 6H). ^{13}C NMR (100 MHz, CDCl$_3$) δ 36.90, 34.73, 34.04, 33.75, 32.14, 31.11, 30.30, 30.27, 29.87, 29.84, 29.73, 29.58, 29.37, 29.16, 26.84, 25.95, 22.91, 14.36.

Alkylation of the 3,6-di(thiophen-2-yl)-2,5-dihydropyrrolo[3,4-c]pyrrole-1,4-dione core (9a-e)

1.5 mmol of 3,6-di(thiophen-2-yl)-2,5-dihydropyrrolo[3,4-c]pyrrole-1,4-dione core are added with 3 eq of anhydrous potassium carbonate to 80 mL of anhydrous DMF and vigorously stirred. 3 eq of the corresponding halogenated side chain (8a-e) are added and the mixture

heated to 100 °C for 12 hours. After the reaction mixture is cooled to room temperature, the DMF is evaporated under reduced pressure, the remnant is dissolved in chloroform (80 mL) and washed with water (2×100 mL), brine (100 mL), and dried of $MgSO_4$. After solvent evaporation, the crude product is purified by column chromatography (hexanes: chloroform 1:1) to yield the desired compound as purple solid.

2,5-bis(4-hexyltetradecyl)-3,6-di(thiophen-2-yl)-2,5-dihydropyrrolo[3,4-c]pyrrole-1,4-dione (9a)

The title compound was recovered as dark purple solid (995 mg, 1.2 mmol, 77%). ^{1}H NMR (400 MHz, $CDCl_3$) δ 8.94 (dd, J = 3.9, 1.1 Hz, 2H), 7.63 (dd, J = 4.9, 1.1 Hz, 2H), 7.31 – 7.23 (m, 2H), 4.06 – 4.00 (m, 4H), 1.80 – 1.64 (m, 4H), 1.37 – 1.16 (m, 62H), 0.91 – 0.79 (m, 12H). ^{13}C NMR (100 MHz, $CDCl_3$) δ 161.44, 140.11, 135.42, 130.73, 129.90, 128.74, 107.79, 42.67, 37.26, 33.65, 32.07, 30.58, 30.22, 29.88, 29.85, 29.80, 29.50, 27.16, 26.82, 26.76, 22.84, 14.28.

2,5-bis(4-octyltetradecyl)-3,6-di(thiophen-2-yl)-2,5-dihydropyrrolo[3,4-c]pyrrole-1,4-dione (9b)

The title compound was recovered as dark purple solid (575 mg, 0.6 mmol, 42%). zz[1]H NMR (400 MHz, $CDCl_3$) δ 8.94 (dd, J = 3.9, 1.1 Hz, 2H), 7.64 (dd, J = 5.0, 1.1 Hz, 2H), 7.32 – 7.24 (m, 2H), 4.07 – 4.01 (m, 4H), 1.76 – 1.63 (m, 4H), 1.38 – 1.15 (m, 70H), 0.90 – 0.80 (m, 12H). ^{13}C NMR (100 MHz, $CDCl_3$) δ 161.39, 140.06, 135.37, 130.69, 129.86, 128.69, 107.74, 42.62, 37.21, 33.60, 30.53, 30.18, 29.83, 29.75, 29.46, 26.77, 26.71, 22.79, 14.23.

2,5-bis(4-decyltetradecyl)-3,6-di(thiophen-2-yl)-2,5-dihydropyrrolo[3,4-c]pyrrole-1,4-dione (9c)

The title compound was recovered as dark purple solid (380 mg, 0.4 mmol, 26%). ^{1}H NMR (400 MHz, $CDCl_3$) δ 8.95 (dd, J = 3.9, 1.1 Hz, 2H), 7.62 (dd, J = 5.0, 1.1 Hz, 2H), 7.30 – 7.25 (m, 2H), 4.07 – 4.00 (m, 4H), 1.77 – 1.66 (m, 4H), 1.35 – 1.18 (m, 78H), 0.88 (t, J = 7.7, 6.1 Hz, 12H). ^{13}C NMR (100 MHz, $CDCl_3$) δ 161.39, 140.07, 135.42, 130.69, 129.89, 128.72, 107.76, 42.66, 37.24, 33.63, 32.06, 30.58, 30.22, 29.85, 29.80, 29.50, 27.16, 26.80, 22.83, 14.27.

2,5-bis(4-decylhexadecyl)-3,6-di(thiophen-2-yl)-2,5-dihydropyrrolo[3,4-c]pyrrole-1,4-dione (9d)

The title compound was recovered as dark purple solid (760 mg, 0.8 mmol, 52%). ^{1}H NMR (400 MHz, $CDCl_3$) δ 8.95 (dd, J = 3.9, 1.1 Hz, 2H), 7.62 (dd, J = 5.0, 1.1 Hz, 2H), 7.31 – 7.24 (m, 2H), 4.08 – 3.99 (m, 4H), 1.77 – 1.64 (m, 4H), 1.42 – 1.15 (m, 86H), 0.88 (t, J = 6.9 Hz, 12H). ^{13}C NMR (100 MHz, $CDCl_3$) δ 161.42, 140.10, 135.43, 130.71, 129.90, 128.73, 107.78, 42.67, 37.25, 33.65, 32.07, 30.59, 30.23, 29.85, 29.81, 29.51, 27.17, 26.81, 22.84, 14.27.

2,5-bis(4-decyloctadecyl)-3,6-di(thiophen-2-yl)-2,5-dihydropyrrolo[3,4-c]pyrrole-1,4-dione (9e)

The title compound was recovered as dark purple solid (815 mg, 0.8 mmol, 50%). ^{1}H NMR (400 MHz, $CDCl_3$) δ 8.96 (dd, J = 3.9, 1.1 Hz, 2H), 7.61 (dd, J = 5.0, 1.1 Hz, 2H), 7.32 – 7.21 (m, 2H), 4.25 – 3.84 (m, 4H), 1.81 – 1.60 (m, 4H), 1.44 – 1.13 (m, 94H), 0.88 (t, J = 6.8 Hz, 12H). ^{13}C NMR (100 MHz, $CDCl_3$) δ 161.30, 139.99, 135.44, 130.60, 129.87, 128.67, 107.72, 42.62, 37.22, 33.62, 32.05, 30.55, 30.21, 29.84, 29.80, 29.50, 29.49, 27.13, 26.79, 22.82, 14.25.

Bromination of the alkylated DPP core (10a-e)

0.5 mmol of the corresponding alkylated DPP (9a-e) were dissolved in 25 mL of chloroform. 2.1 eq. of *N*-bromosuccinimide were added and the reaction refluxed for three hours in the dark. The reaction was quenched by addition of 100 mL of water at room temperature. The organic phase was diluted by addition of 75 mL of chloroform and washed two times with water (2×100 mL) followed by brine (1×100 mL). After separation, the organic phase was dried over MgSO4 and evaporated. The crude product was purified by column chromatography to yield the title compound as a dark purple solid.

3,6-bis(5-bromothiophen-2-yl)-2,5-bis(4-hexyltetradecyl)-2,5-dihydropyrrolo[3,4-c]pyrrole-1,4-dione (10a)

The title compound was recovered as dark purple solid (250 mg, 0.3 mmol, 49%). ^{1}H NMR (400 MHz, CDCl3) δ 8.70 (d, *J* = 4.2 Hz, 2H), 7.24 (d, *J* = 4.2 Hz, 2H), 4.00 – 3.91 (m, 4H), 1.73 – 1.62 (m, 4H), 1.40 – 1.18 (m, 62H), 0.91 – 0.84 (m, 12H). ^{13}C NMR (100 MHz, CDCl3) δ 161.11, 139.12, 135.55, 131.78, 131.23, 119.29, 107.90, 42.74, 37.20, 33.63, 32.08, 30.48, 30.25, 29.90, 29.87, 29.81, 29.52, 27.15, 26.84, 26.78, 22.86, 14.29.

3,6-bis(5-bromothiophen-2-yl)-2,5-bis(4-octyltetradecyl)-2,5-dihydropyrrolo[3,4-c]pyrrole-1,4-dione (10b)

The title compound was recovered as dark purple solid (403 mg, 0.4 mmol, 75%). ^{1}H NMR (400 MHz, CDCl3) δ 8.70 (d, *J* = 4.2 Hz, 2H), 7.24 (d, *J* = 4.2 Hz, 2H), 4.02 – 3.88 (m, 4H), 1.74 – 1.61 (m, *J* = 4.6 Hz, 4H), 1.38 – 1.14 (m, 70H), 0.93 – 0.81 (m, 12H). ^{13}C NMR (100 MHz, CDCl3) δ 161.11, 139.11, 135.55, 131.78, 131.24, 119.29, 107.90, 94.58, 42.74, 37.20, 33.63, 32.08, 30.50, 30.25, 29.87, 29.82, 29.53, 29.52, 27.16, 26.84, 22.85, 14.30.

3,6-bis(5-bromothiophen-2-yl)-2,5-bis(4-decyltetradecyl)-2,5-dihydropyrrolo[3,4-c]pyrrole-1,4-dione (10c)

The title compound was recovered as dark purple solid (379 mg, 0.3 mmol, 67%). ^{1}H NMR (400 MHz, CDCl3) δ 8.70 (d, *J* = 4.2 Hz, 2H), 7.24 (d, *J* = 4.2 Hz, 2H), 4.00 – 3.91 (m, 4H), 1.73 – 1.63 (m, 4H), 1.40 – 1.17 (m, 78H), 0.88 (t, *J* = 6.9 Hz, 12H). ^{13}C NMR (100 MHz, CDCl3) δ 161.11, 139.12, 135.55, 131.78, 131.24, 119.29, 107.90, 42.75, 37.20, 33.63, 32.08, 30.51, 30.25, 29.87, 29.82, 29.52, 27.17, 26.84, 22.85, 14.29.

3,6-bis(5-bromothiophen-2-yl)-2,5-bis(4-decylhexadecyl)-2,5-dihydropyrrolo[3,4-c]pyrrole-1,4-dione (10d)

The title compound was recovered as dark purple solid (338 mg, 0.3 mmol, 57%). ^{1}H NMR (400 MHz, CDCl3) δ 8.70 (d, *J* = 4.2 Hz, 2H), 7.23 (d, *J* = 4.2 Hz, 2H), 3.98 – 3.91 (m, 4H), 1.73 – 1.61 (m, 4H), 1.39 – 1.16 (m, 86H), 0.88 (t, *J* = 6.9 Hz, 12H). ^{13}C NMR (100 MHz, CDCl3) δ 161.04, 139.06, 135.60, 131.76, 131.26, 119.28, 107.87, 42.75, 37.23, 34.82, 34.70, 33.66, 32.12, 31.77, 30.52, 30.28, 29.91, 29.89, 29.85, 29.56, 29.23, 27.17, 27.08, 26.87, 25.43, 22.88, 22.83, 20.83, 14.27, 11.58.

3,6-bis(5-bromothiophen-2-yl)-2,5-bis(4-decyloctadecyl)-2,5-dihydropyrrolo[3,4-c]pyrrole-1,4-dione (10e)

The title compound was recovered as dark purple solid (473 mg, 0.4 mmol, 76%). ^{1}H NMR (400 MHz, CDCl3) δ 8.69 (d, *J* = 4.2 Hz, 2H), 7.21 (d, *J* = 4.2 Hz, 2H), 3.97 – 3.90 (m, 4H),

1.72 – 1.62 (m, 4H), 1.39 – 1.18 (m, 94H), 0.88 (t, J = 6.9 Hz, 12H). ^{13}C NMR (100 MHz, CDCl$_3$) δ 160.99, 139.02, 135.57, 131.74, 131.23, 119.26, 107.82, 42.72, 37.19, 33.63, 32.08, 30.49, 30.25, 29.87, 29.82, 29.52, 27.13, 26.84, 22.85, 14.28.

General polymerization procedure

0.1 mmol of dibrominated DPP monomer (10a-e) was weighted into a 5 mL microwave vial, together with 0.1 mmol of 2,5-bis(trimethylstannyl)thienothiophene, 2 mol% of Pd$_2$(dba)$_3$ and 8 mol% of tri(*o*-tolyl)phosphine and a stirrer bar. [3] The vial was sealed prior to the addition of 4 mL of anhydrous chlorobenzene. The resulting solution was degassed during 30 minutes, before being subjected to microwave heating with the following temperature profile: 2 minutes at 100°C, 2 minutes at 120°C, 5 minutes at 140°C, 5 minutes at 160°C, and 40 minutes at 180°C. The crude polymer was end-capped with trimethyl(phenyl)stannane by heating the polymer solution again for 1 minute at 100°C, 1 minute at 120°C, 2 minutes at 140°C, and 3 minutes at 160°C. The end-capping of the polymer was completed with bromobenzene using the identical heating profile.[4] Residual palladium was chelated by addition of (*E*)-N,N-diethyl-2-phenyldiazene-1-carbothioamide to the solution, which was vigorously stirred at 80ºC in an oil bath during 2 hours.[5] Afterwards, the crude polymer solution was precipitated into methanol, and the resulting dark green polymer fibers filtered into a glass fiber Soxhlet thimble. The polymer was purified by washing with methanol, acetone, and hexane (each for 24 hours) before being extracted from the thimble with chloroform. The polymeric chloroform solution was concentrated on the rotary evaporator and precipitated into methanol. The purified polymer fibers were filtered off and allowed to dry for 48 hours under high vacuum.

The random co-polymer (RCP) was synthesized by weighing 0.096 mmol of 10a and 0.041 mmol of 10e into a 5 mL microwave vial, together with 0.137 mmol of 2,5-bis(trimethylstannyl) thienothiophene, 2 mol% of Pd$_2$(dba)$_3$ and 8 mol% of tri(*o*-tolyl)phosphine and a stirrer bar. This polymerization reaction and purification was conducted following the aforementioned general polymerization procedure.

C$_6$C$_{10}$DPPT-TT: 87 mg of dark green fibrous solid.
M_n = 45 kg.mol^{-1}, M_w = 139 kg.mol^{-1}, Đ$_w$ = 3.1, DP$_n$ = 45.

C$_8$C$_{10}$DPPT-TT: 94 mg of dark green fibrous solid.
M_n = 49 kg.mol^{-1}, M_w = 155 kg.mol^{-1}, Đ$_w$ = 3.2, DP$_n$ = 46.

C$_{10}$C$_{10}$DPPT-TT: 106 mg of dark green fibrous solid.
M_n = 53 kg.mol^{-1}, M_w = 163 kg.mol^{-1}, Đ$_w$ = 3.1, DP$_n$ = 47.

C$_{12}$C$_{10}$DPPT-TT: 115 mg of dark green fibrous solid.
M_n = 51 kg.mol^{-1}, M_w = 162 kg.mol^{-1}, Đ$_w$ = 3.2, DP$_n$ = 44.

C$_{14}$C$_{10}$DPPT-TT: 121 mg of dark green fibrous solid.
M_n = 53 kg.mol^{-1}, M_w = 149 kg.mol^{-1}, Đ$_w$ = 2.8, DP$_n$ = 43.

RCP: 142 mg of dark green fibrous solid.
M_n = 54 kg.mol^{-1}, M_w = 171 kg.mol^{-1}, Đ$_w$ = 3.2, DP$_n$ = 51.
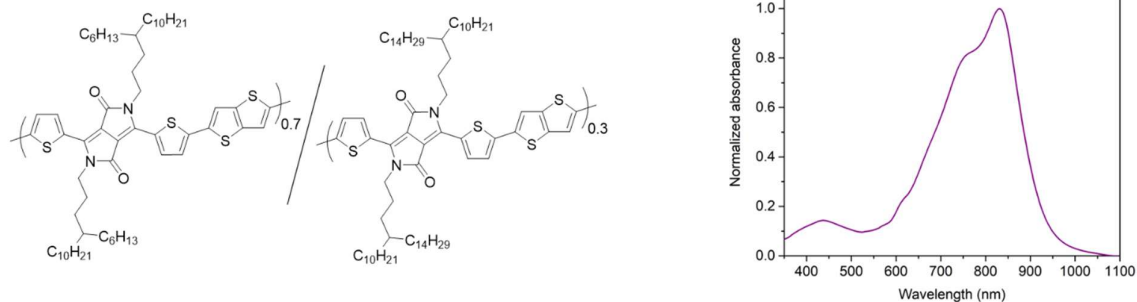
Scheme S2. Chemical structure of the random copolymer **RCP** and the UV-vis. absorption spectrum in thin film, spin-coated at a concentration of 5 mg.mL^{-1} on glass substrate.
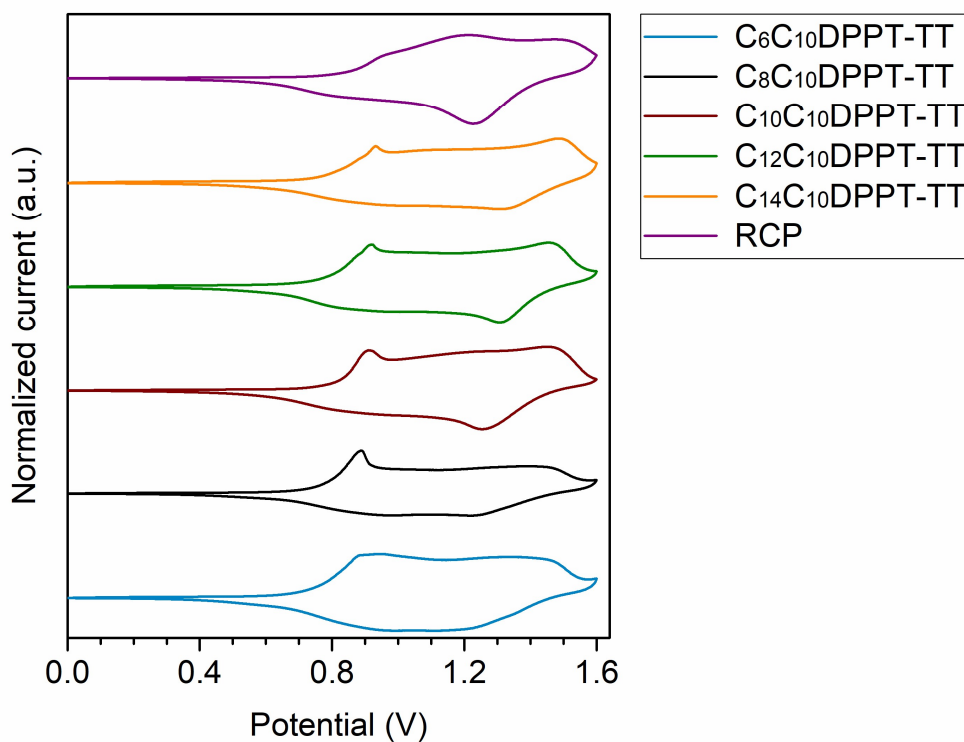
Cyclic voltammetry

Figure S1. Cyclic voltammograms of **C$_x$C$_{10}$DPPT-TT** polymers and **RCP**, dropcast (5 mg.mL^{-1}) from chlorobenzene solutions onto glassy carbon electrodes.
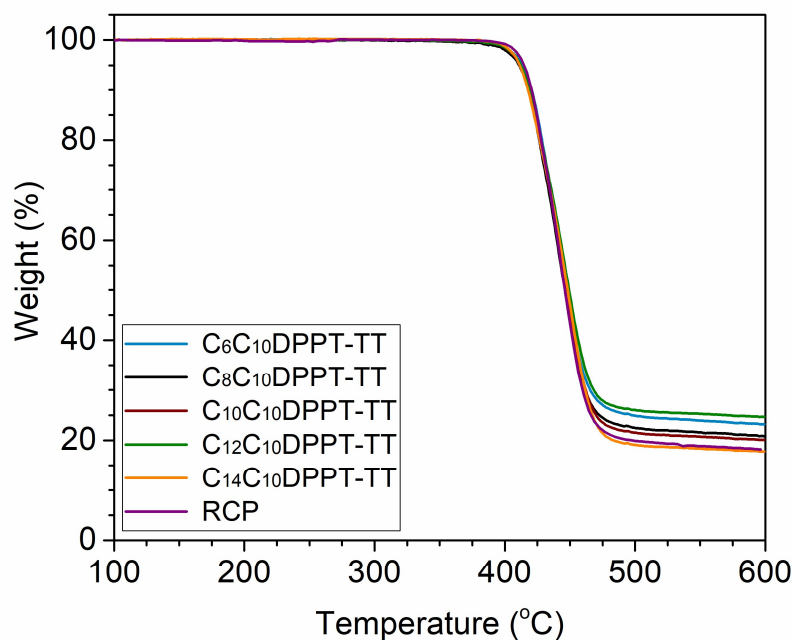
Thermal gravimetric analysis

Figure S2. TGA curves of **C$_x$C$_{10}$DPPT-TT** polymers and **RCP**, recorded under nitrogen flow (40 mL.min^{-1}) at a heating rate of 10°C.min^{-1}.

Differential scanning calorimetry
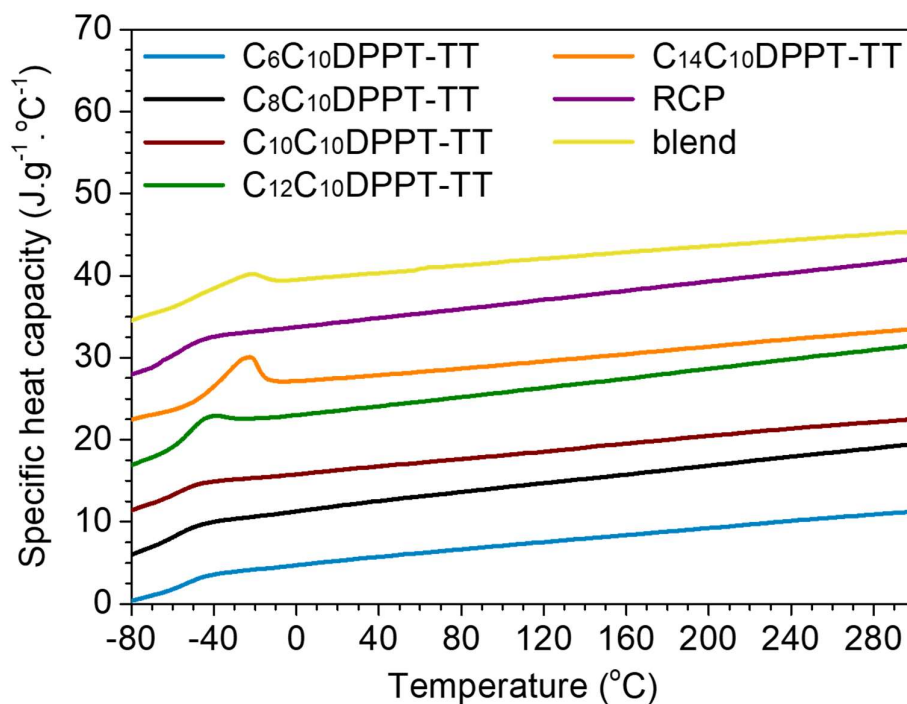
Figure S3. DSC curves of **C$_x$C$_{10}$DPPT-TT**, **RCP** and polymer **blend** respectively. The 2nd heating cycles of all polymers are shown, recorded at 10°C.min^{-1}. Endothermic transitions are positive.

Field effect measurements

An octadecyltrimethoxysilane (OTS) self-assembled monolayer was deposited on highly doped n-type Si <100> wafers with a 300-nm-thick SiO_2 layer according to a previously published literature procedure.[6] The OTS-treated substrate was rinsed subsequently with toluene, acetone, and isopropyl alcohol and dried under a gentle nitrogen stream. The organic semiconductor was spin-coated from a chlorobenzene solution (5 $mg.mL^{-1}$) onto the SiO_2/Si substrates at a spin rate of 1000 rpm for 60 seconds. Thermal annealing of the films was conducted inside a N_2-filled glovebox. Top-contact gold electrodes (40 nm) were thermally evaporated through a shadow mask with the channel length (L) and width (W) defined as 50 and 1000 μm respectively. The transistor characteristics were measured under nitrogen atmosphere using a Keithley 4200 semiconductor parameter analyzer (Keithley Instruments Inc., Cleveland, OH, USA).
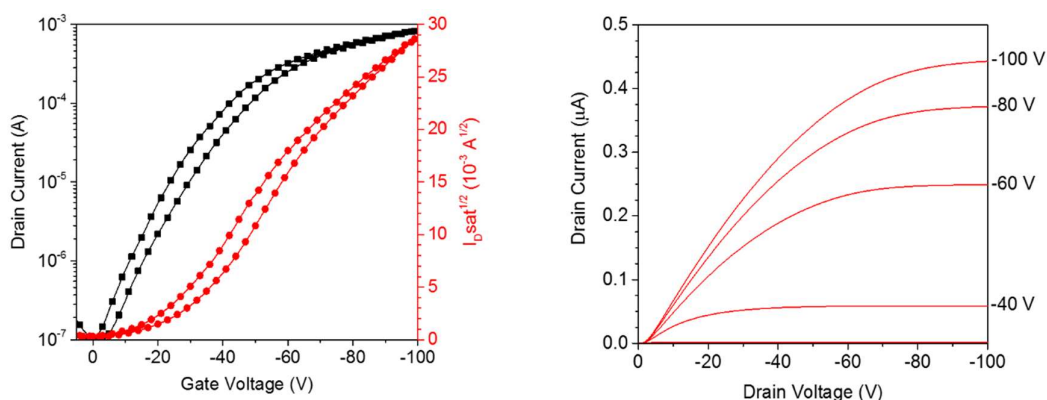
Figure S4. (left) Transfer curve and (right) output characteristics of a BGTC **C₆C₁₀DPPT-TT** based OFET after thermal annealing at 200°C for 1 hour.
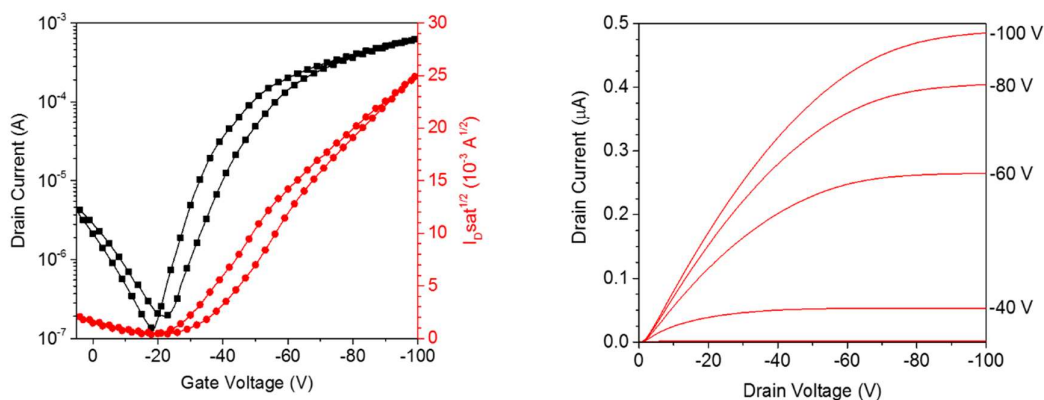

Figure S5. (left) Transfer curve and (right) output characteristics of a BGTC **C₈C₁₀DPPT-TT** based OFET after thermal annealing at 200°C for 1 hour.
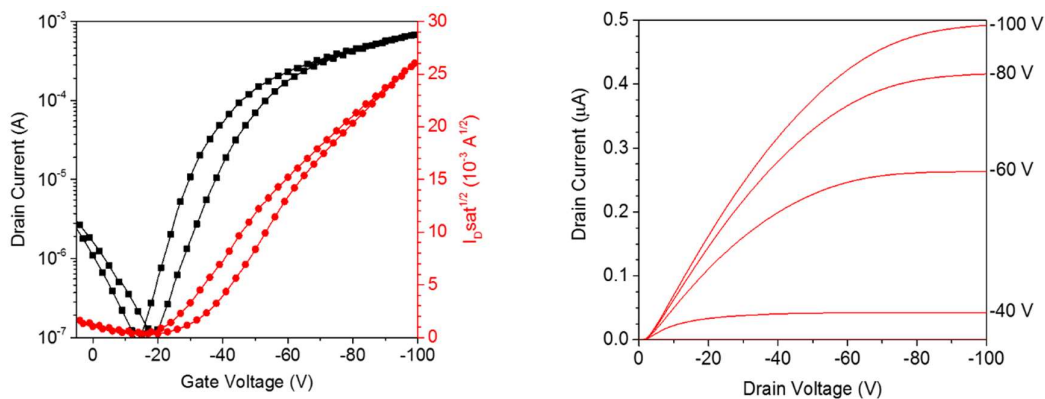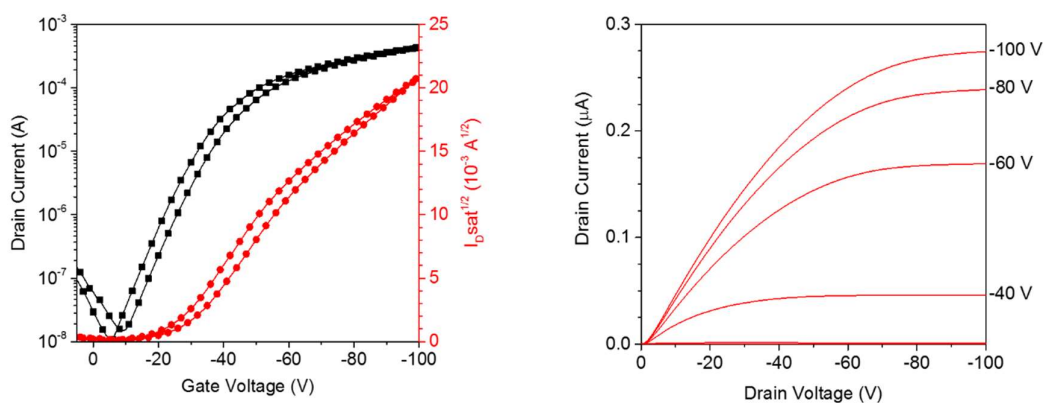
Figure S6. (left) Transfer curve and (right) output characteristics of a BGTC **C₁₀C₁₀DPPT-TT** based OFET after thermal annealing at 200°C for 1 hour.
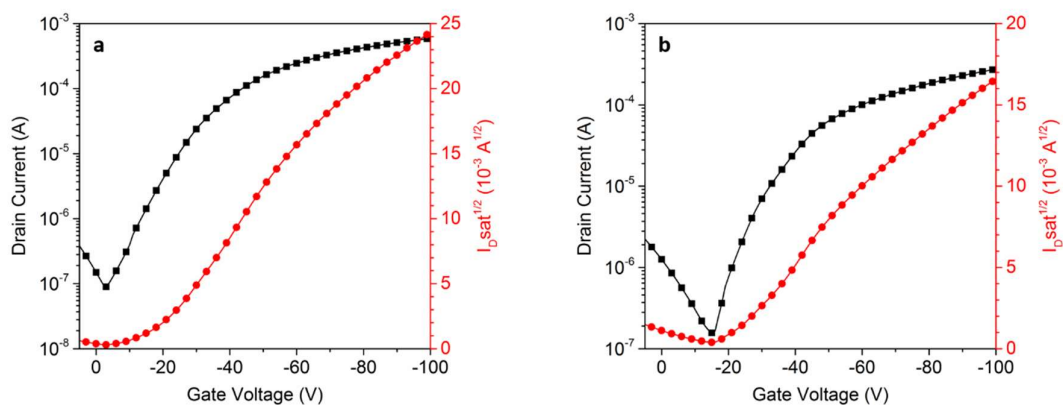

Figure S7. (left) Transfer curve and (right) output characteristics of a BGTC **C₁₄C₁₀DPPT-TT** based OFET after thermal annealing at 200°C for 1 hour.

Figure S8. Transfer curves of a BGTC OFET devices of **C₆C₁₀DPPT-TT** (left) and **C₁₄C₁₀DPPT-TT** (right) after thermal annealing for 20 minutes at 150°C.
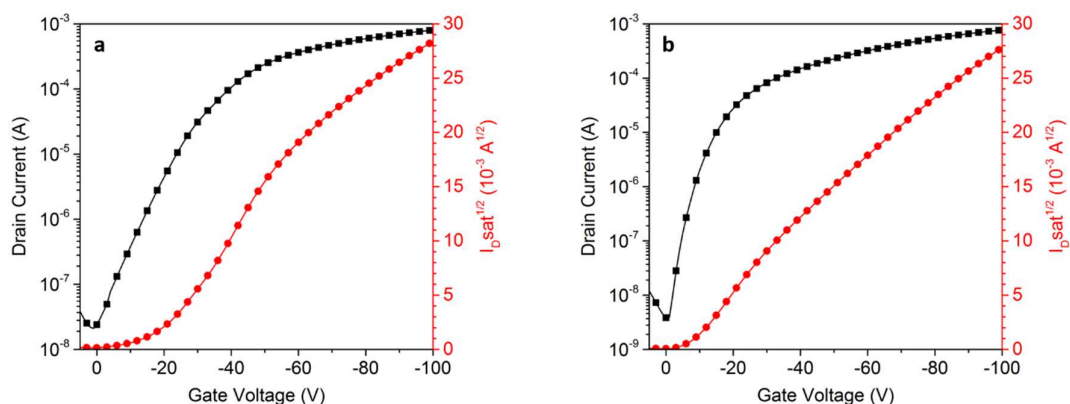
Figure S9. Transfer curves of a BGTC OFET devices of **C₆C₁₀DPPT-TT:C₁₄C₁₀DPPT-TT** blend (7:3) after thermal annealing for 20 minutes at 150°C (left) and for 1 hour at 200°C (right).
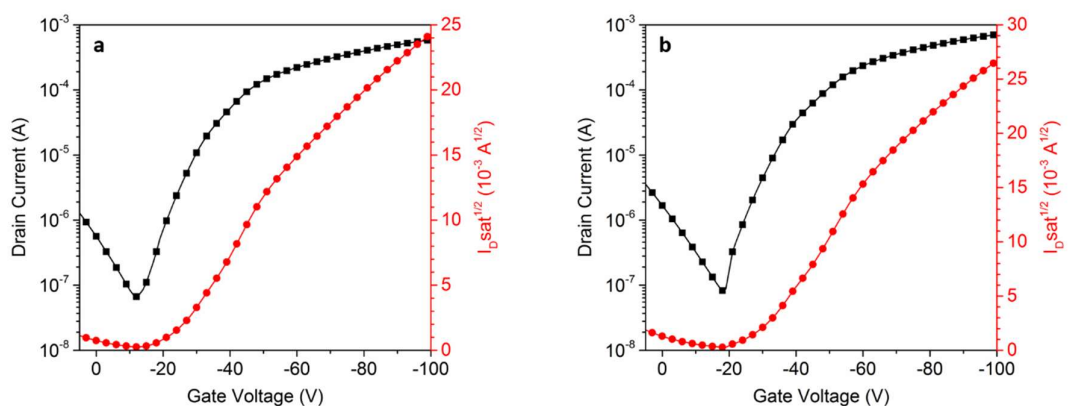

Figure S10. Transfer curves of a BGTC OFET devices of **random co-polymer (RCP)** after thermal annealing for 20 minutes at 150°C (left) and for 1 hour at 200°C (right).

Blend ratio	μ_h^{ave} (cm^{2}V^{-1}s^{-1})	I_{ON}/I_{OFF}^{ave}	V_{th}^{ave} (V)
C₆C₁₀DPPT-TT	2.10± 0.13	3.8×10^4	-19.6± 4.9
70:30	1.52 ± 0.42	8.7×10^4	-4.7 ± 3.7
80:20	1.70 ± 0.48	8.8×10^3	-6.4 ± 5.0
90:10	2.02 ± 0.29	5.5×10^4	-20.7 ± 2.3
C₁₄C₁₀DPPT-TT	1.38± 0.21	7.5×10^4	-19.1± 3.6

Table S1. Summary of the several BGTC OFET characteristics of different **C₆C₁₀DPPT-TT** and **C₁₄C₁₀DPPT-TT** blends, annealed for 1 hour at 200°C.

Polymer	Annealing Temperature (°C)	μ_h^{ave} (cm^{2}V^{-1}s^{-1})	I_{ON}/I_{OFF}^{ave}	V_{th}^{ave} (V)
C$_6$C$_{10}$DPPT-TT	150	1.64 ± 0.35	5.8×10^4	-22.7 ± 4.3
C$_{12}$C$_{10}$DPPT-TT	150	2.16 ± 0.39	2.2×10^4	-19.0 ± 3.6
C$_{14}$C$_{10}$DPPT-TT	150	0.87 ± 0.08	2.5×10^3	-20.3 ± 3.9
blend	150	2.73 ± 0.41	3.5×10^4	-22.8 ± 3.8
RCP	150	2.15 ± 0.40	5.9×10^3	-16.6 ± 4.1
C$_6$C$_{10}$DPPT-TT	200	2.10± 0.13	3.8×10^4	-19.6± 4.9
C$_{12}$C$_{10}$DPPT-TT	200	3.69± 0.42	5.0×10^4	-19.9± 3.3
C$_{14}$C$_{10}$DPPT-TT	200	1.38± 0.21	7.5×10^4	-19.1± 3.6
blend	200	1.52 ± 0.42	8.7×10^4	-4.7 ± 3.7
RCP	200	2.56 ± 0.36	5.4×10^3	-26.5 ± 4.9

Table S1. Summary of the different BGTC OFET characteristics of the different semiconductors and blends, annealed for 20 minutes at 150°C or for 1 hour at 200°C.
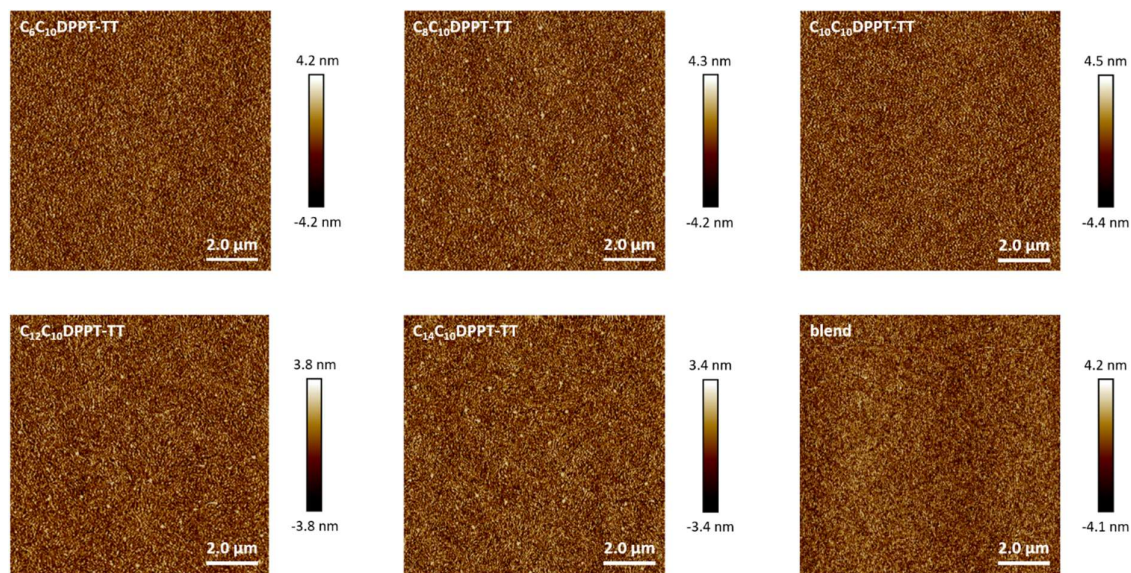
Atomic Force Microscopy

Figure S11. AFM height images of polymer films, spin coated on OTS treated silicon substrates and thermally annealed for 1 hour at 200°C.
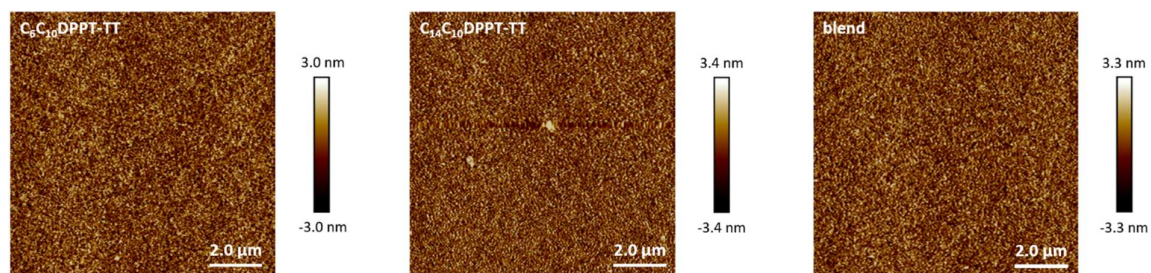

Figure S12. AFM height images of polymer films, spin coated on OTS treated silicon substrates and thermally annealed for 20 minutes at 150°C.
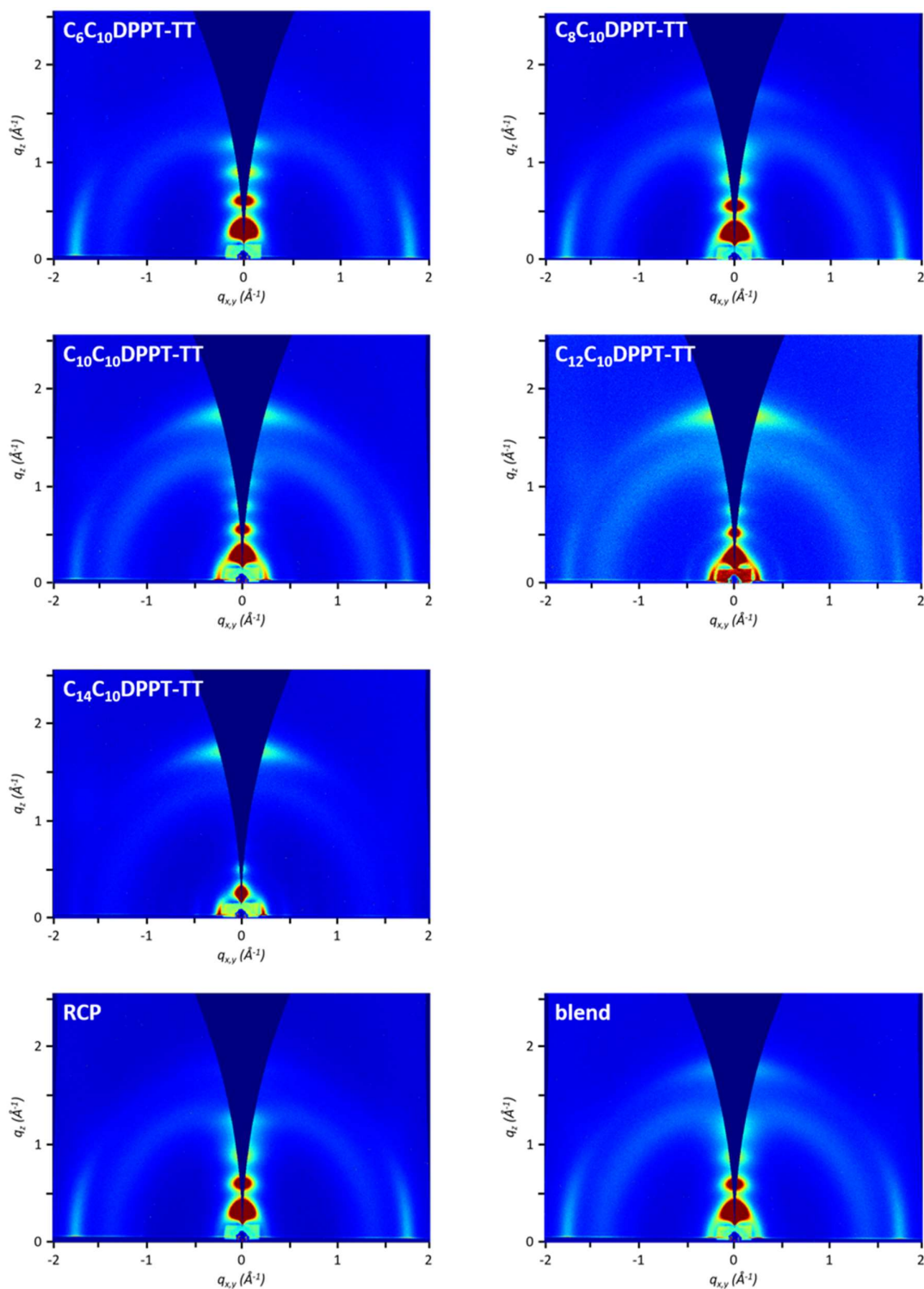
Grazing incidence x-ray diffraction

Figure S13. Grazing incidence X-ray diffraction (GIXD) patterns of the different polymers. The polymer films were spin-coated from 10 mg.mL^{-1} chlorobenzene solutions on Si/SiO2 substrates. The films have been annealed 200°C for 1 hour under a nitrogen atmosphere, with the exception of RCP and blend, which have been annealed at 150°C for 20 minutes.

Calculation of the crystal orientations

The orientation of the crystallites for $C_xC_{10}DPPT$-TT was calculated using the following procedures. The 2-D scattering detector images was first converted into 1-D plot of (010) scattering intensity versus the polar angle χ (Figure S-12). Due to the scattering geometry, a sin χ correction was applied to the raw intensity.[7] The fraction of edge-on vs. face-on was defined by the χ angle as follows: for intensity $-45° < \chi < +45°$, the crystallite orientation is considered face-on dominant, while for $-45° < \chi < -90°$ and $45° < \chi < 90°$, the orientation is edge-on dominant. The corrected scattering intensity was integrated in both regions respectively and compared to obtain their relative fractions.
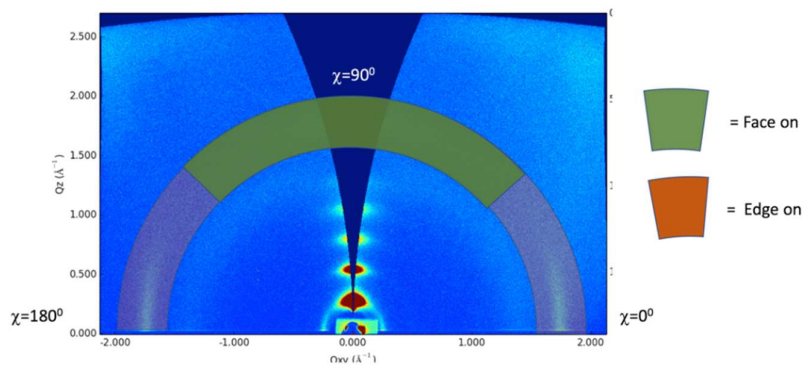

Figure S14. Calculation of relative fraction of edge-on vs face-on ratio of $C_XC_{10}DPPT$-TT crystallites.

Time-of-flight measurements

Capacitor like devices were fabricated by dropcasting $C_xC_{10}DPPT-TT$ solutions (1.5 mg.mL^{-1} in 1,2-dichlorobenzene) inside a nitrogen-filled glovebox onto previously photolithographed indium tin oxide (ITO) glass substrates. An aluminium cathode was then deposited on top of the organic layer via thermal evaporation. Typical device dimensions are 1 μm thick with an area of 4 mm^2, as measured by a Dektak surface profilometer. The devices were annealed at 200°C for one hour, except for the blended device which was annealed at 150°C. The devices were loaded into vacuum chambers while under nitrogen and time of flight (ToF) measurements were carried out under vacuum (10^{-4}–10^{-6} mbar) without ever exposing the samples to ambient atmosphere. The measuring parameters were recorded using an EG101 Lambda Physik gas laser to provide optical illumination. Applied bias voltage was supplied by a DC power supply. The resulting photocurrents were measured as a voltage drop across the 470 Ω input resistance by an Agilent Infiniium digitizing oscilloscope. This was set to average the signal, and background subtraction was carried out on all samples to improve data quality.

Polymer	V/t (V.s^{-1})	Thickness ($\times$ 10^{-8} m)	μ_h^{ave} ($\times$ 10^{-5} cm^{2}V^{-1}s^{-1})
C$_{12}$C$_{10}$DPPT-TT	760.37	6.80E-08	1.25 ± 0.42
C$_{14}$C$_{10}$DPPT-TT	5399.16	4.17045E-08	1.91 ± 0.75
blend	33633.58	1.90943E-08	1.25 ± 0.58

Table S2. Summary of the time-of-flight measurements of the different $C_xC_{10}DPPT-TT$ polymers.

References

[1]   A. B. Tamayo, B. Walker, T.-Q. Nguyen, *The Journal of Physical Chemistry C* **2008**, 112, 11545.
[2]   B. Scheiper, M. Bonnekessel, H. Krause, A. Fürstner, *The Journal of Organic Chemistry* **2004**, 69, 3943.
[3]   S. S. Zalesskiy, V. P. Ananikov, *Organometallics* **2012**, 31, 2302.
[4]   B. C. Schroeder, Y.-C. Chiu, X. Gu, Y. Zhou, J. Xu, J. Lopez, C. Lu, M. F. Toney, Z. Bao, *Advanced Electronic Materials* **2016**, 2, 1600104.
[5]   K. T. Nielsen, K. Bechgaard, F. C. Krebs, *Macromolecules* **2005**, 38, 658.
[6]   Y. Ito, A. A. Virkar, S. Mannsfeld, J. H. Oh, M. Toney, J. Locklin, Z. Bao, *Journal of the American Chemical Society* **2009**, 131, 9396.
[7]   J. L. Baker, L. H. Jimison, S. Mannsfeld, S. Volkman, S. Yin, V. Subramanian, A. Salleo, A. P. Alivisatos, M. F. Toney, *Langmuir* **2010**, 26, 9146.